NATIONAL ENERGY TECHNOLOGY LABORATORY

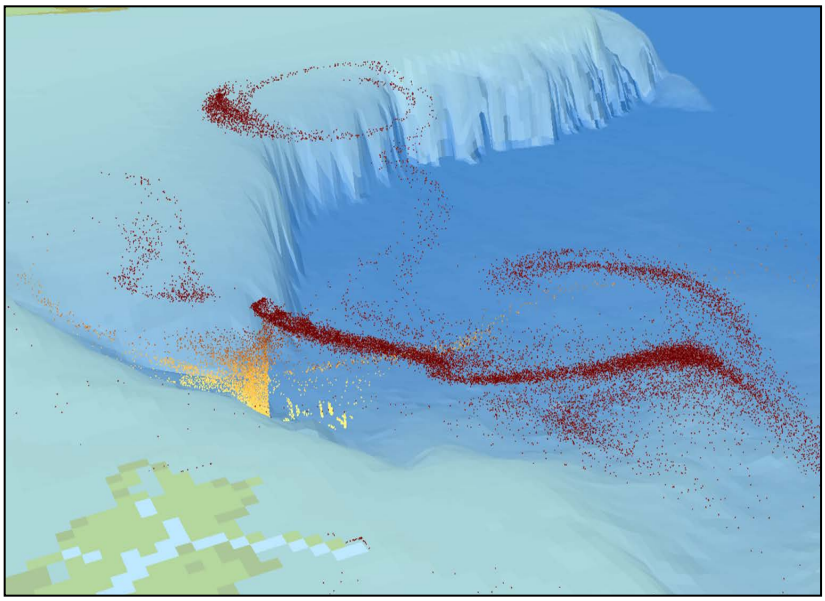

Developing a Comprehensive Deepwater Blowout and Spill Model

7 October 2015

U.S. DEPARTMENT OF ENERGY

Office of Fossil Energy

NETL-TRS-9-2015

Disclaimer

This report was prepared as an account of work sponsored by an agency of the United States Government. Neither the United States Government nor any agency thereof, nor any of their employees, makes any warranty, express or implied, or assumes any legal liability or responsibility for the accuracy, completeness, or usefulness of any information, apparatus, product, or process disclosed, or represents that its use would not infringe privately owned rights. Reference therein to any specific commercial product, process, or service by trade name, trademark, manufacturer, or otherwise does not necessarily constitute or imply its endorsement, recommendation, or favoring by the United States Government or any agency thereof. The views and opinions of authors expressed therein do not necessarily state or reflect those of the United States Government or any agency thereof.

Cover Illustration: 3-D image of spill particles from IASNFS (Intra-America Seas Nowcast Forecast System) run on May 20, 2010 rendered in ArcScene. Image is looking southeast from Mississippi Delta; vertical exaggeration is set at 20; particles are colored from reddish-brown to bright yellow the deeper they are. Visible is the main rising jet/plume, the oil plume extending up De Soto Canyon (left), and an oil plume tail curling and extending south-southwest (towards viewer-right).

Suggested Citation: Sim, L.; Graham, J.; Rose, K.; Duran, R.; Nelson, J.; Umhoefer, J.; Vielma, J. *Developing a Comprehensive Deepwater Blowout and Spill Model*; NETL-TRS-9-2015; EPAct Technical Report Series; U.S. Department of Energy, National Energy Technology Laboratory: Albany, OR, 2015; p 44.

An electronic version of this report can be found at:

http://www.netl.doe.gov/research/on-site-research/publications/featured-technical-reports

https://edx.netl.doe.gov/offshore

Developing a Comprehensive Deepwater Blowout and Spill Model

Lawrence Sim[1], James Graham[2], Kelly Rose[1], Rodrigo Duran[1,3], Jake Nelson[1,4], Joe Umhoefer[1,5], Jason Vielma[1]

[1] U.S. Department of Energy, Office of Research and Development, National Energy Technology Laboratory, 1450 Queen Avenue SW, Albany, OR 97321

[2] Geography Department, Humboldt State University, 1 Harpst Street, Arcata, CA 95521

[3] College of Earth, Ocean, and Atmospheric Sciences, Oregon State University, 104 CEOAS Administration Building, Corvallis, OR 97333

[4] College of Computing and Infomatics, Drexel University, 30 North 33rd Street, Philadelphia, PA 19104

[5] Department of Mathematics, Oregon State University, Kidder Hall 368, Corvallis, OR 97331

NETL-TRS-9-2015

7 October 2015

NETL Contacts:

Kelly Rose, Principal Investigator

Lawrence Sim, Technical Coordinator

Cynthia Powell, Focus Area Lead

This page intentionally left blank.

Table of Contents

ABSTRACT **1**

1. INTRODUCTION **2**

2. NEAR-FIELD JET **4**

3. CRUDE OIL AND GAS/HYDRATES **8**

4. SPILL TRANSPORT AND WEATHERING **10**

5. HYDRODYNAMIC HANDLER AND ADDITIONAL DETAILS **14**

6. MODEL VALIDATION **17**

7. CONCLUSIONS **22**

8. REFERENCES **23**

APPENDIX A: CONTROL-VOLUME AND ENTRAINMENT **A-1**

APPENDIX B: DROPLET-SIZES AND TERMINAL BUOYANT VELOCITY **B-1**

APPENDIX C: TURBULENT DIFFUSION **C-1**

APPENDIX D: WEATHERING MODELS **D-1**

Appendix C was added to this paper after the final revisions by coauthors, several mistakes in this appendix were subsequently found. Please disregard the Appendix C and refer to the technical report by Duran (2016) for the diffusion schemes used in BLOSOM.

Duran, R. *Sub-Grid Parameterizations for Oceanic Oil-Spill Simulations*; NETL-TRS-9-2016; EPAct Technical Report Series; U.S. Department of Energy, National Energy Technology Laboratory: Albany, OR, 2016; p 36.

List of Figures

Figure 1: Generalized model of spill immediately following a blowout event highlighting the important components of offshore spill originating from seafloor sources including i) the buoyant jet, ii) potential for gas separation, iii) the potential for gas hydrate formation, iv) terminal level where the jet devolves into v) individual particle or droplets, vi) submerged plumes, and vii) the surfaced oil slick..... 3
Figure 2: Representation of an oil/gas jet composed of a series of control-volumes. 4
Figure 3: Simplified diagram of forces affecting an individual control-volume. 5
Figure 4: Generalized schematic of weathering and degradation processes currently accounted for in BLOSOM. 12
Figure 5: Simplified schematic of BLOSOM components and interactions. 15
Figure 6: Example of BLOSOM's current graphical user-interface..... 16
Figure 7: Comparison of jet/plume from BLOSOM until reaching terminal level against observations from North Sea field experiment 17
Figure 8: Results from simulation on IASNFS pictured at May 20, 2010. The background is colored by sea surface speed, black dots represent surfaced particles, grey dots represent submerged plumes, and the magenta represents the EMPSR spill extent layers which is both filled-in behind and outlined over the particles for enhanced clarity. 19
Figure 9: Results from simulation on GOM HYCOM pictured at May 20, 2010. 20
Figure 10: 3-D image of spill particles from IASNFS run on May 20, 2010 (same data as Figure 8) rendered in ArcScene. Image is looking southeast from Mississippi Delta; vertical exaggeration is set at 20; particles are colored from reddish-brown to bright yellow the deeper they are. Visible is the main rising jet/plume, the oil plume extending up De Soto Canyon, and an oil plume tail curling and extending south-southwest. 21

Acronyms, Abbreviations, and Symbols

Term	Description
3-D	Three-dimensional
BLOSOM	Blowout and Spill Occurrence Model
CDOG	Clarkson Deepwater Oil and Gas
CSV	Comma-separated values
EKE	Eddy kinetic energy
EMPSR	Experimental Marine Pollution Surveillance Report
FVCOM	Finite-Volume Community Ocean Model
GIS	Geographic information system
GNOME	General NOAA Operational Modeling Environment
GOM	Gulf of Mexico
GOR	Gas-to-oil volume ratio
GUI	Graphical user-interface
HYCOM	Hybrid Coordinate Ocean Model
IASNFS	Intra-America Seas Nowcast Forecast System
NCOM	Navy Coastal Ocean Model
NOAA	National Oceanic and Atmospheric Administration
ROMS	Region Ocean Modeling System
TSV	Tab-separated values
d	Diameter (m)
d_0	Diameter of blowout (m)
Fr	Froude number
g	Acceleration due to gravity (9.8 m s^{-2})
h	Height or slick thickness (m)
j	Jet coefficient
M	Molar mass (g mol^{-1})
m	Mass (kg)
m_Q	Mass entrained (kg)
P	Pressure (Pa)
P_v	Vapor pressure (Pa)
K	Eddy diffusion coefficient (m^3)
K_{EKE}	Eddy kinetic energy (m^2s^{-2})
K_S	Eddy diffusivity from Smagorinsky (m^2s^{-1})
Q	Entrained volume flux (m^3)
Q_s	Volume flux due to shear-entrainment (m^3)
Q_f	Volume flux due to forced-entrainment (m^3)
R	Gas constant (8.314 J K^{-1} mol^{-1})
Re	Reynolds number
r	Radius (m)
T	Temperature (K)

Acronyms, Abbreviations, Symbols (cont.)

Term	Description
t	Timestep length (s)
V	Volume (m^3)
$\vec{\mathbf{v}}$	Velocity ($m\ s^{-1}$)
v	Component speed ($m\ s^{-1}$)
u	x-axis/zonal speed ($m\ s^{-1}$)
v	y-axis/meridional speed ($m\ s^{-1}$)
w	z-axis/vertical speed ($m\ s^{-1}$)
w_b	Terminal buoyant velocity ($m\ s^{-1}$)
We	Weber number
$\Delta\rho$	Density deficit ($kg\ m^{-3}$) of the hydrocarbons subtracted from ambient
δ	Droplet-size/diameter (m)
δ_{50}	Median droplet-size (m)
δ_C	Critical diameter (m)
ρ	Density ($kg\ m^{-3}$)
σ	Interfacial tension ($N\ m^{-1}$), sometimes standard deviation
τ	Lagrangian timescale (s)
μ	Dynamic viscosity ($Pa\ s^{-1}$)

Acknowledgments

This work was performed as part of the National Energy Technology Laboratory (NETL) research for the U.S. Department of Energy's (DOE) Complementary Research Program under Section 999 of the Energy Policy Act of 2005. Funding was provided in part by the Bureau of Safety and Environmental Enforcement, U.S. Department of the Interior, Washington, DC, under agreement E14PG00045; and the College of Earth, Ocean, and Atmospheric Sciences at Oregon State University. Open libraries used in BLOSOM's development include SchoonerTurtle's BlueSpray (http://schoonerturtles.com), EJML (http://ejml.org), GDAL/OGR (http://gdal.org), GeoTools (http://geotools.org), and UCAR's NetCDF (http://unidata.ucar.edu).

This page intentionally left blank.

ABSTRACT

BLOSOM (Blowout and Spill Occurrence Model) is a complete and stand-alone modeling package for the simulation of deepwater blowout and spill scenarios from source to final fate and degradation. BLOSOM is flexible in its construction and utility, coupling the methodologies from traditional, particles-based spill and weathering models with recent research in jet/plume modeling and adapts all processes to be three-dimensional (3-D) and spatially-explicit. Evaluations against the North Sea Field Experiments as well as the Deepwater Horizon Spill showcase its capabilities at simulating both surface spill extents and submerged oil plumes. Major spill features were identified in the simulated results as well as the presence of submerged oil plumes corresponding to available observations. Results suggest an ensemble approach with multiple hydrodynamic models to assess agreements and discrepancies between predictions.

1. INTRODUCTION

Traditionally, oil spill models have focused heavily on surface spill behavior and tracking. As a result, they have lacked an integrated, explicit three-dimensional (3-D) subsea-surface element. Yet the 3-D behavior of multi-phase hydrocarbon released from the seafloor and the dynamics of buoyant jets and oil plumes predicates the ultimate fate and transport of the resulting spill (Figure 1). In the past, this deficiency was largely mitigated by the fact that most offshore exploration was constrained to relatively shallow-water settings. Even with a seafloor-sourced spill, an adequate estimation of the surfacing location and mass or volume-flux could be entered into a surface-focused model as if it were a surface source spill with relative confidence.

As offshore hydrocarbon development activities pushed into deeper waters, the need to explicitly address the 3-D nature and role of submerged plumes grew considerably, particularly highlighted by Deepwater Horizon Spill, with a mixture of oil and gases emanating from the Macondo Prospect wellhead at over 5,000 ft (>1,500 m) of depth. In addition, the response protocols further emphasized the need to not only track hydrocarbon on the sea surface but throughout the water column. Vast volumes of the spill never surfaced from the Deepwater Horizon Spill—over 40% according to some estimates (McNutt et al., 2011). At least one study found a subsurface plume more than 35 km in length constituting 6% or more of the total amount of oil released following the Macondo incident (Camilli et al., 2010) and another indicated heavy amounts of settled hydrocarbons on the seafloor directly adjacent to the well head (Valentine et al., 2014). In addition to improving estimates of flow rate, understanding of the ultimate transport and fate of hydrocarbons throughout offshore systems, including within the water column, is a critical need for deeper water systems.

Buoyant-jet models for oceanic applications were initially developed for offshore sewage discharges and similar outfall systems. Lee and Cheung (1991) developed JETLAG (short for Lagrangian jet) with such applications in mind, using Lagrangian control-volume elements that moved in space and simulated the volume of all fluids inside as a singular element. As each control-volume moved through the water-column, it accumulated ambient water from both shear and forced entrainment, increasing its size, decreasing its buoyancy, and generally decreasing its momentum—though also potentially gaining momentum, especially in strong cross currents that would bend the jet over to the side. JETLAG and other similar models provided the framework for oil and gas blowout modeling and with some adaptations led to the development of models such as CDOG (Clarkson Deepwater Oil and Gas) (Zheng et al., 2002) and DeepBlow (Johansen, 2000). Yapa and Zheng (1997) began by incorporating gases into the control-volumes. A number of other developments followed including gas separation from a bent jet/plume (Chen and Yapa, 2004; Johansen, 2000), droplet-size estimations (Chen and Yapa, 2007; Johansen, 2002), hydrate formation and decomposition (Johansen, 2000; Yapa et al., 2001), terminal buoyant velocity calculations (Zheng and Yapa, 2000), and gas dissolution (Zheng and Yapa, 2002), among others. Meanwhile, traditional spill models improved by factoring in vertical processes such as dispersion, the breakup of surface slicks into subsurface droplets by wave action, and the adoption of a pseudo-components approach to oil weathering. Other advances came from increased computational power and improved algorithms.

Each of these approaches targeted part of a large, integrated system for offshore hydrocarbon fate and transport. What remained then was the challenge of combining all these recent developments, particularly the merging of two different modeling approaches: control-volumes of mixed fluids and gases for jet/plume models and a particles-based approach used in many

spill-transport models. BLOSOM (Blowout and Spill Occurrence Model) addresses this need by merging and advancing existing sub-system modeling approaches, to produce an integrated, 3-D, and spatially-explicit, blowout-system spill model in a singular suite. BLOSOM performs as a singular model to the user, while operating beneath the hood as a multi-component modeling framework.

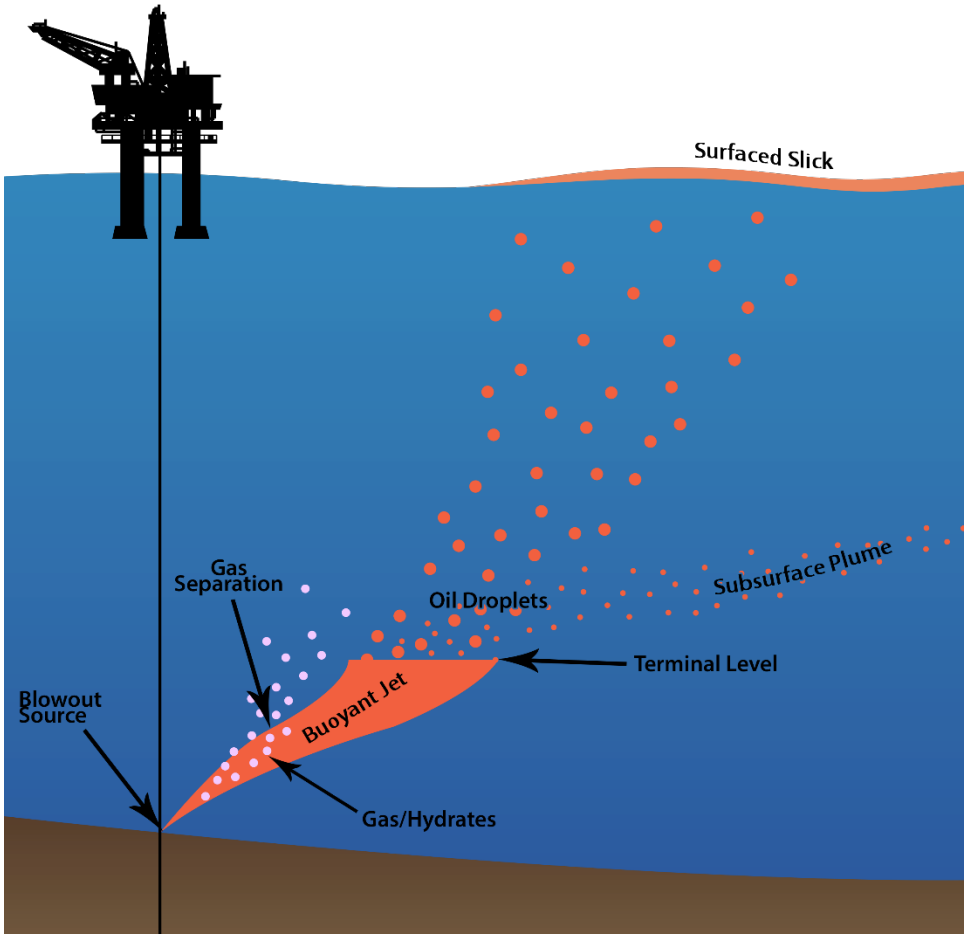

Figure 1: Generalized model of spill immediately following a blowout event highlighting the important components of offshore spill originating from seafloor sources including i) the buoyant jet, ii) potential for gas separation, iii) the potential for gas hydrate formation, iv) terminal level where the jet devolves into v) individual particle or droplets, vi) submerged plumes, and vii) the surfaced oil slick.

2. NEAR-FIELD JET

BLOSOM employs and integral model to simulate the near-field jet, employing Lagrangian control-volume analysis which models the near-field buoyant jet as a conceptual volume of mixed hydrocarbons, gases, and entrained water (Lee and Cheung, 1991). This can be visualized by stacking cylindrical, cross-sectional slices throughout the jet that move upward and expand (Figure 2). The physics of each control-volume are largely controlled by momentum and buoyancy, and change is primarily driven through the entrainment of ambient water into the control-volume. As water is entrained, the volume and mass must be appropriately adjusted, but with this also comes a shift in density and momentum. The control-volume's change in mass occurs from a positive change due to entrainment of ambient water and some mass loss due to separation of gas bubbles and gas dissolution (Figure 3), while change in momentum is due to the entrained momentum and acceleration due to buoyancy (Equation 2a). The control-volumes are assumed to be non-interfering and cylindrical in shape. Control-volumes in BLOSOM always maintain a fixed orientation with the horizontal plane and shear due to horizontal displacement, as opposed to bending control-volumes, which turn to match the direction of the movement.

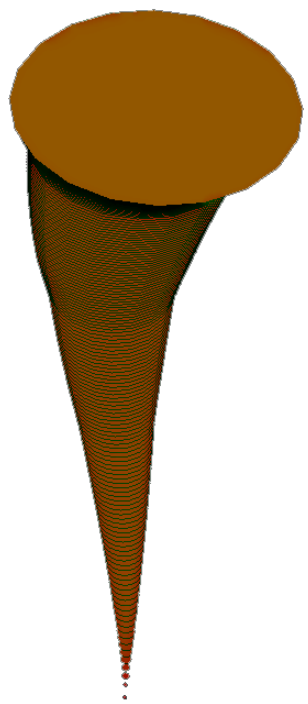

Figure 2: Representation of an oil/gas jet composed of a series of control-volumes.

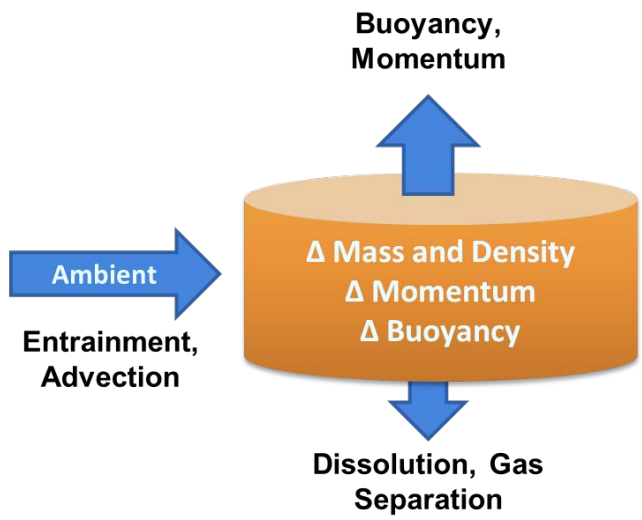

Figure 3: Simplified diagram of forces affecting an individual control-volume.

Meanwhile, the change in height of the control-volume is calculated as a function of the change in velocity, which in turn drives the change in width to maintain the proper volume. Thus as a control-volume slows, for example, the control-volume will flatten out and expand. When the control-volume nears the terminal-level however, it tends to exaggerate the effect of thinning and in situations with less entrainment, the control-volume acts as if almost unaffected by ambient currents. Thus the jet coefficient (j) was created to adjust the behavior of the control-volume more like a droplet-cloud as it approaches an intermediate-phase. The jet-coefficient ranges from 0.0 (acting more as a cloud of individual droplets driven by buoyancy and advection) to 1.0 (acting completely as a momentum-dominated jet with full entrainment) and is calculated as a hyperbolic tangent function of the difference in the control-volume's velocity from the ambient velocity projected onto it.

$$j = \tanh(a\pi|\vec{\mathbf{v}} - \vec{\mathbf{v}}'_{\mathrm{a}}|) \tag{1}$$

where $\vec{\mathbf{v}}$ is the control-volume's velocity; $\vec{\mathbf{v}}'_a$ is the magnitude of the ambient velocity projected onto $\vec{\mathbf{v}}$; and the coefficient a is a fitting parameter, for which a value of 5.9 was used based on simulations against the North Sea Field Experiments.

The change in height is linearly scaled by the jet coefficient so that as the jet coefficient approaches 0, height is assumed to be constant. Similarly, the speed for some component of the velocity at the next-timestep before adjustment (v'_{k+1}) is adjusted with the jet coefficient to be more strongly influenced by advection (Equation 2b).

$$\mathrm{v}'_{n+1} = \frac{(m_n - m_L)\mathrm{v}_n + m_Q \mathrm{v}_a}{m_{n+1}} + \frac{\Delta\rho}{\rho_n} g t \boldsymbol{k} \tag{2a}$$

$$\mathrm{v}_{n+1} = \mathrm{v}'_{n+1} + (1 - j^2)(\mathrm{v}_a + w_b \boldsymbol{k} - \mathrm{v}'_{n+1}) \tag{2b}$$

where the subscript n indicates values at the last timestep; m_Q is mass entrained and m_L mass lost; v is a component of the velocity in some axis direction; v_a is the speed of the ambient fluid in that direction; w_b is the terminal buoyant velocity; ρ is density of the control-volume and $\Delta\rho$ the density deficit, or the difference between the ambient and the control-volume; g is acceleration due to gravity; t is the length of the timestep; and $\boldsymbol{k}$ is a unit vector in the upwards direction – that is, buoyancy and terminal buoyant velocity is only a factor in the z-axis and ignored in x or y-axis calculations.

Lee and Cheung (1991) modeled the dynamics of a buoyant plume through shear and forced entrainment for which the basic equations are unchanged except for a slight adjustment for non-bending control-volumes. Shear entrainment is due to the boundary conditions of the control-volume element and the ambient fluid, which occurs regardless of ambient currents. Forced entrainment is due to cross-flow conditions (i.e. ambient currents directly forcing entrainment into the control-volume). More detailed information on the calculation of the jet can be seen in Appendix A.

Theoretically, the total entrained mass equals the sum of the volume-fluxes entrained multiplied by the ambient density. However, full entrainment is unlikely—especially as the jet becomes less momentum-dominated, and BLOSOM uses the jet-coefficient again to regulate mass entrained as shown below, where Q_f is the calculated volume of forced entrainment and Q_s is the same for shear entrainment.

$$\frac{dm_Q}{dt} = j\rho_a \left(\frac{dQ_f}{dt} + \frac{dQ_s}{dt} \right) \tag{3}$$

One of the major drivers of non-surfacing plumes is the distribution of droplet-sizes, as most crudes are less dense than seawater, even in their heavier components. Droplet-sizes are proportional to the terminal buoyant velocity, meaning that smaller droplet-sizes rise more slowly and are more easily trapped by turbulence, much like heavier-than-air particulates may be suspended by turbulence in the air. Previously, and in the simulations to follow, the maximum droplet-size was calculated using a formula based on the blowout diameter and the Weber number (Rye et al., 1996) capped to a user-defined maximum, and the distribution of droplet-sizes assumed to follow a Rosin-Rammler distribution with the value of coefficients changing depending on the gas-to-oil volume ratio (GOR) as described by Johansen (2002). Dispersants were simulated by manually “capping” the maximum droplet-size parameter. In the newest version of BLOSOM, a median droplet-size is calculated from the relationship between a modified Weber number and the Reynolds number as described by Johansen et al. (2013) in which dispersants effects are best simulated by scaling down the given crude oil viscosity. GOR is accounted for by using the void ratio to modifying the exit velocity and calculation of the Froude number. Droplet-size distributions are still calculated by means of a Rosin-Rammler distribution. Further details are available in Appendix B.

To calculate the terminal buoyant velocity, a three-phase approach for spherical, ellipsoidal, and spherical-cap regimes is used as described in Zheng and Yapa (2000). Particles with a diameter of 1 mm or less are assumed to be spherical in shape while those with a diameter between 1 mm and the critical diameter are assumed to be ellipsoidal, and all particles above the critical diameter are assumed to be spherical-cap in shape.

BLOSOM simulates a singular control-volume at a time, creating a new one only when the active control-volume reaches the terminal level. At that point, the conditions of and the fluxes of the terminal level are updated to be accessed by the far-field model as needed and a new control-volume is created at the blowout source. By accounting for the mass as a mass flux and correcting for changes in the time to reach the terminal-level, this saves some computational time from creating a control-volume every timestep. The terminal level is assumed to be reached when either the control-volume reaches the water surface; the jet-coefficient drops below 0.5, or when the vertical velocity of the control-volume is nearly equal to the calculated terminal buoyant velocity calculated for the oil droplets.

While the approach taken by using Lagrangian control-volumes simplifies the jet/plume in a control-volume relatively accurately, it does make the assumption that the gas bubbles are rising at a similar rate or that ones that escape above are simply replaced by the control-volume below. However, gas bubbles will naturally rise faster than the liquid portions of the plume due to buoyancy, and in strong cross-currents this creates an uneven horizontal displacement by depth, meaning that due to the slip-velocity between the gas bubbles and the liquid, gas bubbles will leak and peel off in strong cross-currents. Assuming that the bubbles though randomly dispersed within the control-volume are evenly dispersed, the model calculates the displacement of the control-volume and the equally-sized gas extent in the control-volume. The volume of the gas-core no longer intersecting the control-volume is then multiplied by the original gas-fraction of the jet/plume to obtain the volume of gas to have separated from the plume. The process is adapted from the method described in Chen and Yapa (2004). While methane may present a hazard to response if present in significant quantities at the surface, for purposes of this model all gases are ignored once leaving the control-volume as in deepwater conditions it is assumed that most gases will undergo significant, if not total, dissolution before surfacing.

3. CRUDE OIL AND GAS/HYDRATES

While some models handle crude properties as a set of mostly-static parameters, BLOSOM includes separate models for both the crude (liquid hydrocarbons) and the gases for enhanced detail. Crude oils are not handled as a conglomerated entity with averaged physical properties, but split up into pseudo-components, each of which can be independently monitored or their properties averaged as needed. This provided a better fit with the pseudo-components approach to evaporation and allowed a more detailed picture of the exact composition of the crude in the output data. Gases are handled similarly—as a mixture of gases within the gas/hydrate model, but with averaged properties as needed.

Crude oil properties are loaded or defined as distillation cuts with associated volume or mass fractions, vapor temperatures, and specific gravities. For each pseudo-component, molecular mass, molar volume, and pseudocritical temperature and pressure are approximated using the correlations given by Kesler and Lee (1976) and Twu (1984). Densities are calculated separately for each pseudo-component using the Spencer-Danner (modified Rackett) method with COSTLAD correction for pressure as described in Chang et al. (2012). The densities of all the pseudo-components are then volume-averaged (with the emulsified water content) to give an overall density for the crude, which allows for more accurate handling of changes to crude property as different components experience different rates of weathering and degradation. Changes to viscosity are handled via an empirical correlation from Mackay et al. (1982) as a function of temperature using a reference measurement of oil viscosity that also exponentially increases with evaporation and water-content (due to emulsification).

If gases are present, they are assumed to be well-mixed in gas bubbles within the bulk hydrocarbon phase, and the compressibility factor is solved with the Brill and Beggs (1973) correlation for gas mixtures. When properties of individual gases must be known, the Peng-Robinson equations of states are used to determine the compressibility factor and fugacity with a volume translation as described in Baled et al. (2012) to correct for discrepancies in high pressure environments.

Maximum stable gas bubble-sizes are determined by the energy dissipation rate and interfacial-tension as described in Bandara and Yapa (2011). On exceeding the maximum stable bubble-size as gases expand due to reduced pressure, the bubble-size is assumed to be the same as the calculated maximum stable bubble-size. To calculate the slip velocity, a harmonic mean approach of two different slip velocity calculations are used as described in Johansen (2000). The slip-velocity—while it can be ignored in weak cross-flow conditions under the assumption that gas leaving the control-volume is simply replaced from the control-volume below—plays a large role in the separation of gas bubbles in strong cross flows.

Gas dissolution is calculated using the method described in Zheng and Yapa (2002) for which the dissolution rate is based off of solubility and the mass transfer coefficient is calculated based on the bubble size-regime. To obtain the solubility, the modified Henry's law from King (1969) as described in Zheng and Yapa (2002) is solved with a known fugacity (from the Peng-Robinson equation of state).

At great depths, high pressures and low temperatures may allow for the formation of gas hydrates, ice-like structures of water and gas (particularly those formed from methane and ethane), which are assumed to form a thin shell around the gaseous bubbles. Due to the heat and mass transfers associated with hydrate formation and decomposition, the dynamics of hydrates

may have significant effects on the behavior of the jet, particularly by increasing the overall density of the control-volume (Yapa et al., 2001). BLOSOM uses the hydrate kinetics model of Englezos et al. (1987a,b) with the approach described in Yapa et al. (2001) to incorporate the resulting heat and mass transfers. In BLOSOM, hydrates are calculated for methane and ethane, using the model proposed by Englezos et al. (1987a) where the difference in this fugacity from three-phase equilibrium drives both formation and decomposition. In the case of hydrate formation, gases formed into hydrates are removed from the mixture and stored separately, while decomposed hydrates are assumed to be dissolved and discarded from the system. Due to hydrate formation and dissolution of gases, the mixture must be readjusted at every timestep, requiring a recalculation of the pseudocritical properties and average molar mass.

4. SPILL TRANSPORT AND WEATHERING

Proper conversion methods are necessary to break up the control-volume into separate particles, each with different physical and chemical properties, to account for the widths the jet/plume can reach once arriving at a terminal level and the generalizations made in a control-volume analysis. Failure to consider complexities of this transition could account for a major cause of plumes that peel off and do not surface, as the control-volume includes a varied distribution of droplet-sizes. Thus, the conversion module is an important transitional linkage between the control-volume-based jet/plume model and the particle-based transport model. The conversion model oversees the conversion of a spatially explicit 3-D volume into spatially explicit points in 3-D space, taking care to account for the distribution of hydrocarbon masses and droplet-sizes in the control-volume.

Droplet-size classes are created spanning from some user-specified minimum to maximum droplet-size. By default, the minimum droplet-size is set to 20 microns and the maximum the same as the enforced maximum droplet-size of 10 mm. This was chosen to best capture the different droplet-size behaviors observed in the modeling efforts of North et al. (2011), which found droplet-sizes at or below 50 microns to have good agreement with measured subsurface plumes during the Deepwater Horizon. Fractions of the total crude mass accumulated at the terminal level are split according to the droplet-size classes and turned into individual particles with the appropriate mass distributions using the Rosin-Rammler droplet-size distribution. Otherwise the crude is assumed to be well-mixed and all other properties are the same. Droplets are assumed to expand as they rise due to decreasing pressure.

Lagrangian discrete parcels are used to simulate particles which may represent an oil slick or droplet cloud within the water column, with oil slicks assumed as a circular area with some thickness on the water surface and droplet clouds as an ellipsoid boundary in which oil droplets are present in some concentration. The main means of transporting oil in the far-field is through forcing from currents and if the parcel has surfaced, winds and wave energy. Combined with existing hydrodynamic models, hydrocarbon fate and transport are determined for each particle at every timestep to determine its new drift velocity (Shen et al., 1987). Vertical velocities are a sum of advection by the vertical currents as well as the calculated terminal buoyant velocity for the mean droplet-size given to the parcel (see Appendix B for calculations).

Wind advection, which is user-specified, is usually a few percent of the 10 m surface wind velocity (Madsen, 1977) and is deflected according to the method described by Wang et al. (2005). The experience the National Oceanic and Atmospheric Administration (NOAA) has gathered with their computer assisted response and restoration simulations suggests an empirical value for wind advection ranging from 1–4% (see GNOME [General NOAA Operational Modeling Environment] technical manual). However, many of the 3-D primitive equation ocean models (e.g. ROMS [Region Ocean Modeling System], NCOM [Navy Coastal Ocean Model], FVCOM [Finite-Volume Community Ocean Model], HYCOM [Hybrid Coordinate Ocean Model]) already include a parameterization of Ekman dynamics in the ocean’s near-surface, and as such, little-to-no wind advection may be adequate (Durksi, 2004, 2015).

Turbulent horizontal diffusion can be simulated in a number of ways, which potentially holds the largest effect on the fate of the particles besides the currents themselves. There exists two methods available in BLOSOM for computing the eddy diffusivity values necessary for modeling diffusion, either by means of advective velocity variance experienced by the parcels or

the eddy viscosity from the Smagorinsky (1963) model. The velocity variance approach takes the sample variance (σ^2) of the Lagrangian velocity the particle experiences throughout its trajectory, from which the Lagrangian eddy kinetic energy (EKE) is computed, whereas the Smagorinsky model calculates eddy viscosity from the Eulerian velocity gradients at the particle's current location as shown below.

$$K_{EKE} = 0.5(\sigma_u^2 + \sigma_v^2) \tag{4}$$

$$K_S = C_s \Delta x \Delta y \sqrt{\left(\frac{\partial u}{\partial x}\right)^2 + \frac{1}{2}\left(\frac{\partial v}{\partial x} + \frac{\partial u}{\partial y}\right)^2 + \left(\frac{\partial u}{\partial y}\right)^2} \tag{5}$$

Where K_{EKE} is diffusivity calculated as EKE (in units of m^2s^{-2}); K_S is eddy diffusivity calculated from the Smagorinsky model for subgrid eddy viscosity (in units of m^2s^{-1}); σ^2 is the sample velocity variance with (u, v) denoting speeds in the zonal and meridional directions respectively; $\Delta x \Delta y$ are the grid sizes and together represents the grid area; and C_s is the Smagorinsky coefficient, by default set to 0.15.

The Smagorinsky model is mostly spatially dependent, with temporal dependence tied to intervals of the hydrodynamic solutions used, as well as explicitly tied to the resolution of the hydrodynamic solution used. Meanwhile, the EKE approach is very temporally dependent on the parcel's lifespan and somewhat less explicit in the spatial dependence. Due to the way EKE is approximated, the sensitivity of EKE can be much more pronounced initially while becoming increasingly stable over multiple timesteps. Potentially, this may increasingly feedback on itself due to a high diffusive velocity and escalating variance as it rapidly changes location as a consequence of its overestimated stochastic movement. To avoid such a case in BLOSOM, a minimum of 10 timesteps must be reached before returning an EKE value, otherwise diffusion is assumed to be null initially. Consequently, the results of each method scale quite differently—by one or more orders of magnitude and thus the diffusion scheme must have specific methods to calculate the diffusive velocity for each approach.

Random-walk for spill modeling is based on Fisher et al. (1979) wherein a random diffusion velocity is added to every particle at each timestep as a function of a random number generator and the diffusivity. It is the simplest of the methods as a zeroth-order Markov model with each step being completely independent. Random-flight (Heemink, 1990) is a first-order Markovian processes that incorporates memory in the velocity perturbations, scaled by a Lagrangian timescale (τ) which effectively determines the length of time for two adjacent particles to develop uncorrelated diffusive velocities. The timescale usually ranges from one to several days and must be set by the user based on knowledge of the region and ocean patterns. The final possible approach is a hybrid method which incorporates a first-order Markovian process for the magnitude of the diffusive velocity, much like the random flight model, but with the directional component perturbed by independent increments not tied to the time scale. Further details are available in Appendix C.

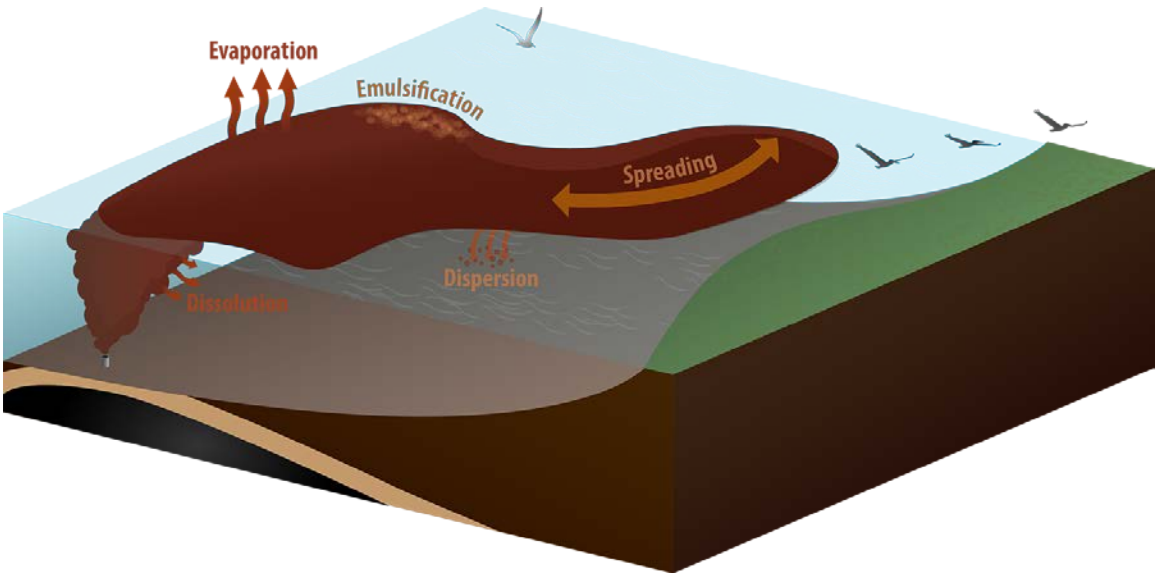

Figure 4: Generalized schematic of weathering and degradation processes currently accounted for in BLOSOM.

A visual overview of the weathering processes currently included in BLOSOM can be seen in Figure 4. Evaporation is by far the largest degradative process for the crude oil. Combined with the crude oil handling described previously, evaporation is computed for each pseudo-component which allows each pseudo-component to evaporate independently and disproportionately. When the components are re-averaged to obtain the total crude properties, an increase of density and loss of mass should result, with the former due to the general nature of lighter components to evaporate more expediently.

Emulsification, as opposed to evaporation, increases the volume of the sea surface slick by foaming oil and water into a mousse-like emulsion, spurred by the turbulent action of waves (Reed et al., 1999). Emulsification both inhibits evaporation and can increase viscosity by two to three-fold (Lehr, 2001). Using recent research by Fingas and Fieldhouse (2003, 2004, 2012), the presence of resins and asphaltenes are used to determine the emulsion's stability class and associated maximum water content. These are combined with equations for time to formation as a function of the stability class and local wave height.

Dispersion is the breaking up of the sea surface slick through wave action, forcing droplets to break from the surface slick and entrain back into the water column. These droplets may rise immediately causing little change; they may rise slowly, by which time the surface slick has moved horizontally, creating the tail-like spreading effect seen in many oil slicks; or they may not rise at all, instead being too small for their buoyant velocity to overcome turbulent, vertical motion. The model for the volume of oil dispersed into the water column as a function of droplet-size is given by Delvigne and Sweeney (1988). For droplets that will not surface, dispersion is assumed lost and degraded (most likely through dissolution and biodegradation although kept in a "dispersion" category). In BLOSOM, dispersion is only calculated for those droplets that are assumed lost and degraded.

Dissolution, while relatively insignificant compared to other degradation processes, can play an increasingly larger role over large periods of time, especially for subsurface plumes that lack

many other means of degradation. Thus, for submerged plumes, dissolution is calculated for each pseudo-component through the model described in Riazi and Roomi (2008) and adjusted with the fraction of the component being composed of aromatics, if such data is available, which have a higher solubility. For surfaced slicks, the crude is assumed to preferentially evaporate over dissolve, thus no dissolution is assumed to occur.

Biodegradation, the degradation of crude oil by microbial communities, is a relatively slow process that nevertheless plays an important role in the long-term fate of hydrocarbons. While not implemented in oil spill models, they could be quite significant to the oil budget in extreme spills, as the Macondo Spill proved (Camilli et al., 2010). However, modeling biodegradation is marred by complexities due to different hydrocarbon components, different bacterial consortiums, and the influences of a plethora of environmental factors, including but not limited to temperature, oxygen, nutrients, and pressure (Atlas, 1981). As such, while biodegradation is planned for future capability in BLOSOM, it is not currently included. Instead, parcels that have degraded from other means below some minimum mass are removed and the mass assumed biodegraded.

Spreading is handled using the original equations by Fay (1971) for the gravity-viscosity phase, and also modeled indirectly through an increased number of particles and horizontal diffusion, both of which tend to separate highly clustered slick parcels in a particles-based scale.

Expanded descriptions of the weathering and degradation models are listed in Appendix D.

5. HYDRODYNAMIC HANDLER AND ADDITIONAL DETAILS

In the simplest configuration, BLOSOM uses fixed conditions with the only variability being pressure (and in-situ density) by depth. The next format allows a user to upload a custom table of currents, temperatures, and salinities by depth, giving variance on the vertical axis (but still assuming fixed on the horizontal planes). The most complex is through the use of outputs from hydrodynamic models provided as netCDFs. A handler component designed to accommodate outputs from any of the plethora of hydrodynamic models allows BLOSOM to incorporate an ocean model the user is most familiar with or prefers. In that light, the hydrodynamic handler for BLOSOM was designed for flexibility with the various data formats outputted by different hydrodynamic models.

Support for unstructured and structured grids both are in place, with the handler using a windowed quad-tree algorithm for quick searching of nodes and elements in unstructured grids. This has been tested successfully on outputs from NCOM, HYCOM, and FVCOM, as well as adapted to read the existing GNOME standard. Values are interpolated linearly by depth and can be interpolated on the horizontal plane either bilinearly (for structured grids) or through inverse-distance weighting (for unstructured), or not at all. Bathymetry data, which may or may not be provided with the hydrodynamic dataset, may also be supplanted by a user-selected dataset for greater resolution.

In-situ densities, specific heats, viscosities, and interfacial tensions for the ambient seawater are calculated with a series of empirical correlations as provided by Fofonoff and Millard (1983) and Sharqawy et al. (2010). The hydrodynamic handler is also equipped with algorithms to perform some basic vector field calculations such as gradients, divergence, and curl, through which it can obtain horizontal diffusivities based on the Smagorinsky (1963) model for eddy diffusivity. For estimating wave heights and periods where necessary and if not supplied, the model uses equations for correlating by wind speed and fetch, assuming a mean between an unlimited fetch and duration correlation versus fetch-limited, with fetch obtained from grid size or nodal distance.

Vertical velocities, if not provided, are estimated from the horizontal volume divergence at the nearest layer and given a random multiplier from -1 to 1, similar to the random-walk procedure used for horizontal diffusion. A future implementation will be able to compute a diagnostic vertical velocity and direction by integrating the divergences and the incompressibility condition through all the depths and boundaries.

Dispersants are not presently modeled by BLOSOM, but a similar effect can be forced by specifying a much lower maximum droplet-size than the default, e.g. by lowering the figure by a factor of 5 to 10 or more. This will force the droplet-sizes to be capped by such a maximum and have that maximum similarly applied in the droplet-size distribution. However coefficients in the distribution equation are unchanged. Alternatively, a parameter may be input to lower the value of the crude’s viscosity. However a direct model for estimating this with the dispersant-to-oil ratio, likely a figure much easier to obtain, does not yet exist. The effects of the presence of dispersants themselves to weathering processes are not yet modeled although many degradation processes will naturally benefit from the increased surface area to volume ratio with smaller droplets.

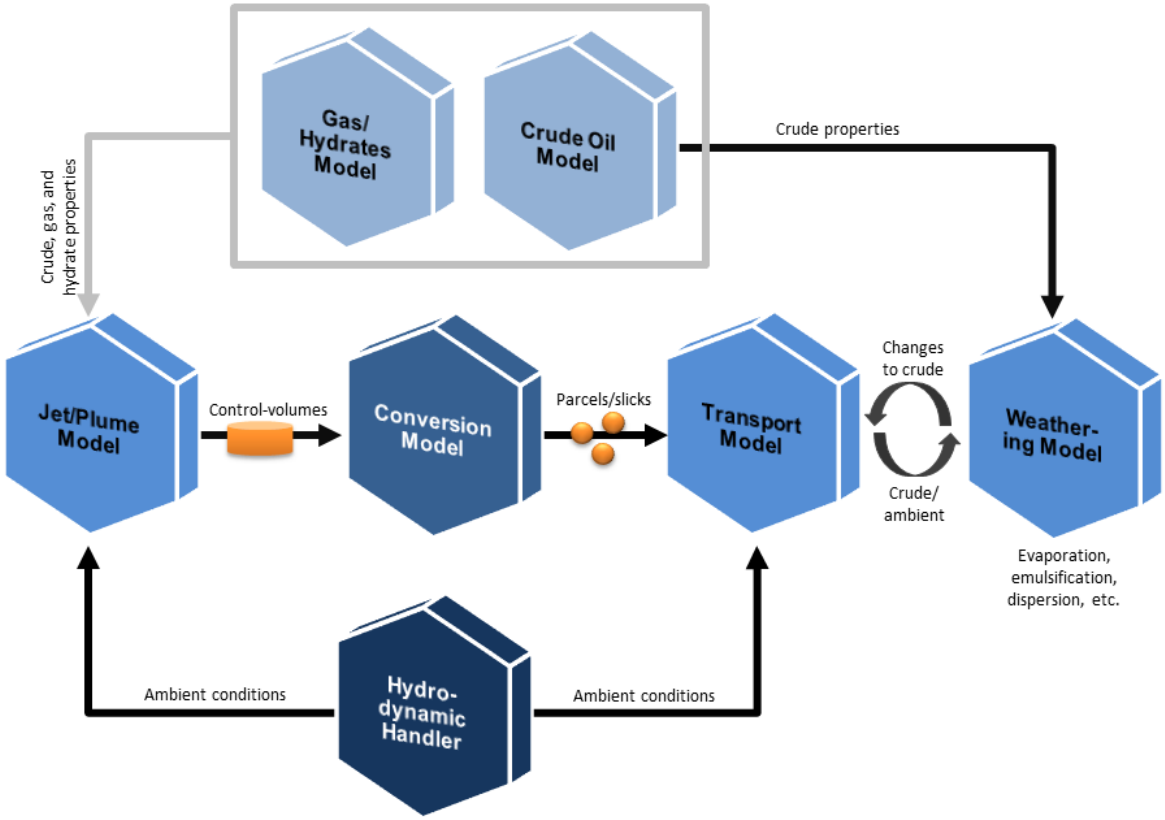

Figure 5: Simplified schematic of BLOSOM components and interactions.

Each of BLOSOM's components work more or less independently, but also as a unified framework that brings everything together into a flexible but cohesive, integrated-system model as depicted in Figure 5. BLOSOM is built on the Java language, allowing for flexibility across multiple platforms and operating systems. This also allows for the use of Java's concurrency libraries to optimize particle simulations. This becomes particularly useful for the simulation of particles, which can easily number in the tens-to-hundreds-of-thousands in long simulations, allowing for processing of multiple particles simultaneously to expedite simulation through a timestep.

BLOSOM may be run either through a graphical user-interface (GUI) (Figure 6) or through scripts. The GUI includes a basic geographic information system (GIS) to visualize spill results, and spatial coordinates and coordinate-systems are explicitly handled. As all spatial calculations are based in meters, BLOSOM enforces a projected coordinate system with unit meters for the model to run on. However, as hydrodynamic data often comes in geographic coordinate systems, necessary methods to convert between coordinate systems are in place.

Outputs may be given in a tabular format (e.g. CSV [comma-separated values], TSV [tab-separated values], or Excel spreadsheet) with spatial locations specified in appropriate columns but otherwise limited metadata, or given as a geographic shapefile with all attributes and

metadata provided in the format. Basic spill statistics are accumulated as BLOSOM runs, which can be visualized graphically in the BLOSOM interface (Figure 6), saved to a table, or saved as an image. All outputs can be user-specified to be saved automatically at regular intervals as the simulation runs. Additionally, entire scenarios may be saved and loaded, as well as previous outputs reloaded into the BLOSOM interface to continue the simulation from where it ended last.

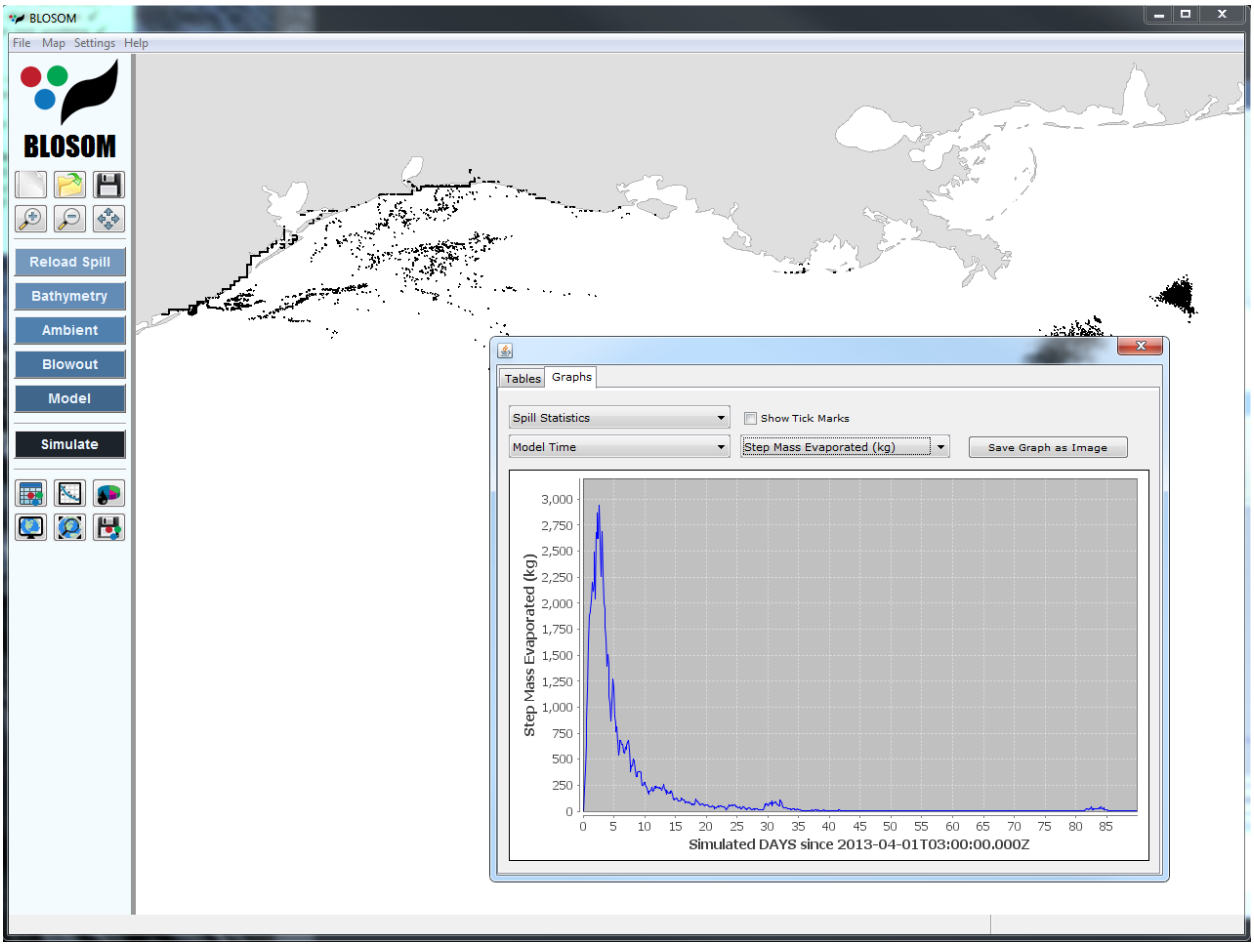

Figure 6: Example of BLOSOM's current graphical user-interface.

6. MODEL VALIDATION

As "[v]erification and validation of numerical models of natural systems is impossible" (Oreskes, 2010; Oreskes et al., 1994), common usage of these terms in the scientific literature often result in a misleading sense of truth which is important to avoid in policy applications (Sterman et al., 1994). However, evaluation of models is essential for testing, understanding the model's strengths and limitations, and gaining confidence in its capabilities.

While opportunities for evaluating blowout and oil-spill models are rare, a series of field experiments conducted in the North Sea (Rye et al., 1996) are commonly compared against to evaluate the near-field portions of blowout models. The jet/plume component of BLOSOM ran simulations emulating these field-experiments for a rough comparison. The terminal-level, simulated at almost exactly 55 m depth, match well with observations that saw an end to "jet-like" behavior between 50–60 m depth (Rye and Brandvik, 1997) and the widths of the jet coincide nicely—especially noting the sudden expansion between 70–80 m depth (Figure 7). The largest discrepancy occurs in the horizontal displacement of the jet, but this may be attributed to the coarse current data collection (every 30 m depth), as this discrepancy occurred in other oil/gas jet model validations as well (Yapa et al., 1999).

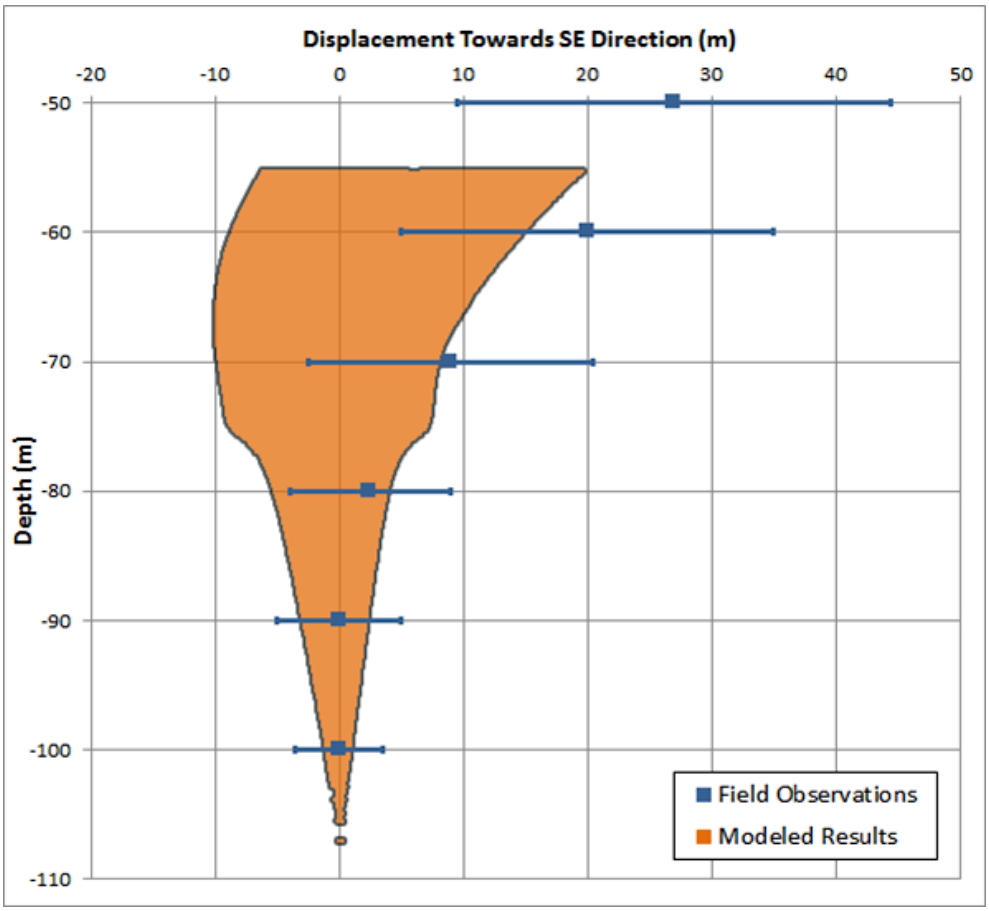

Figure 7: Comparison of jet/plume from BLOSOM until reaching terminal level against observations from North Sea field experiment (Rye and Brandvik, 1997).

To demonstrate the far-field capabilities of BLOSOM, simulations were performed against the Deepwater Horizon Spill, notable for having sufficient observational data for a cursory model evaluation. The blowout was initialized on May 6, 2010, using satellite observation data to place 25,000 particles more-or-less randomly around the delineated spill extent then run until the May 20, 2010 with the blowout continuing to add mass to the jet/plume model throughout the entire run. This placed the simulation within the period when the distinct "tiger-tail" appeared, around mid-May. Observed spill extent data used to initialize and compare against were provided from NOAA's Experimental Marine Pollution Surveillance Report (EMPSR), a product created from a composite of remotely-sensed data (available at http://www.ssd.noaa.gov/PS/MPS/deepwater.html).

Nowcasts from two different operational hydrodynamic models were used. The first was the IASNFS (Intra-America Seas Nowcast Forecast System) implementation of NCOM (Navy Coastal Ocean Model) with a spatial resolution of 1/24° and a temporal resolution of 6-hrs (provided by the Northern Gulf Institute at http://www.northerngulfinstitute.org). While a newer implementation of NCOM with even greater resolutions exists, nowcasts from that model began on the May 25, 2010 and could not be used. The second model used was the Gulf of Mexico (GOM) regional implementation of HYCOM (Hybrid Coordinate Ocean Model) with a spatial resolution at 1/25° and a much coarser temporal resolution of 24-hrs (available at https://hycom.org). Wind advection was left out for both model runs and the model timesteps were set at 10 min. For horizontal diffusion schemes, the simplest method of random-walk employed.

The results on the May 20, 2010, 2 weeks after initialization with no mid-run corrections, are shown in Figure 8 and Figure 9. While the results from both simulations have divergences, they also have overall similarities, and both show the growth of the "tiger-tail" as observed, although the run using the GOM HYCOM shows the tail extending much further south constituting the larger discrepancy. This is not surprising given the poor temporal resolution in HYCOM data and the trajectories' sensitivity to time-dependence. However, the results from HYCOM agree well with the modeled outputs of Le et al. (2012) using the same ocean data and hold a stronger match with the spill extent data from Roffer's Ocean Fishing Forecasting System (http://www.roffs.com/deepwaterhorizon.html) (not shown), a proprietary nowcast which incorporated more expert-knowledge and in-situ observations to extend the spill extent beyond what could be discerned from remote-sensing alone. IASNFS, while at a higher given spatial resolution, appears to have modeled the currents at a coarser scale, blurring many of the sub-mesoscale eddies and general turbulence, as evidenced in the figures. The IASNFS run deviated somewhat from observations by predicting a dominant westward movement of the spill. Even with these limitations it is remarkable that both ocean models were able to replicate many of the major features of the observed spill.

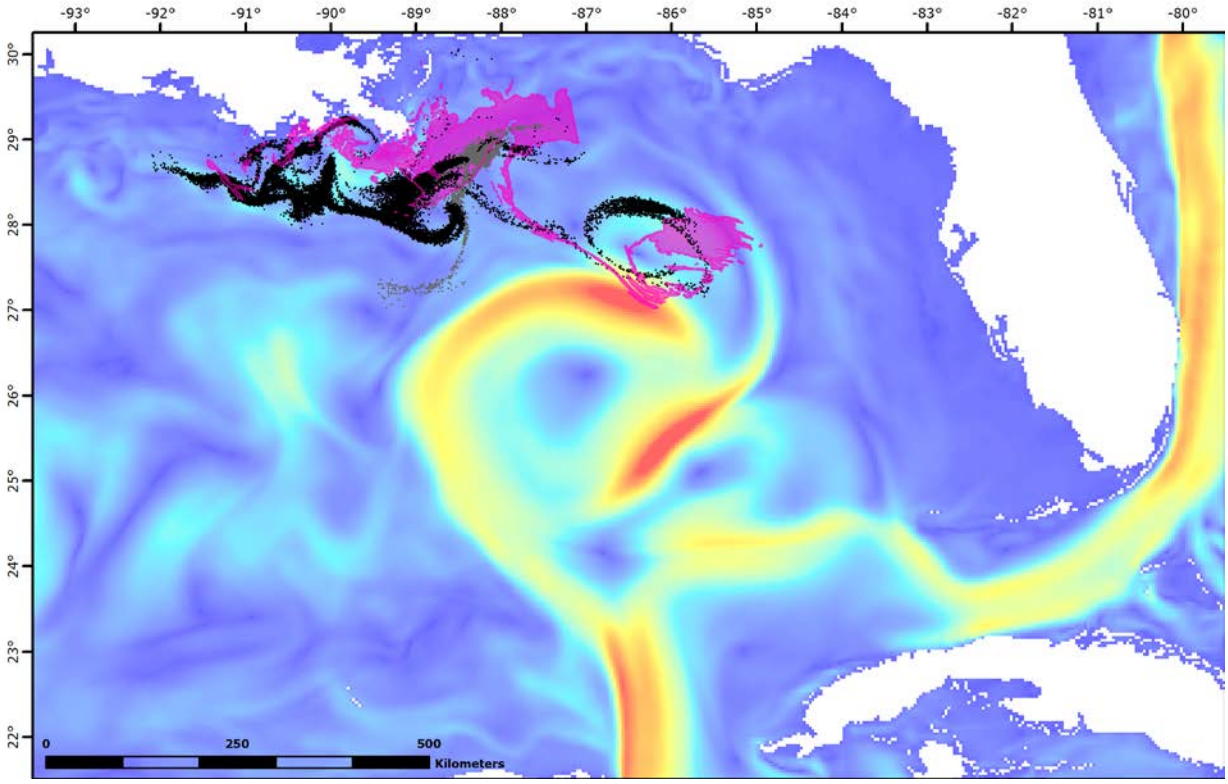

Figure 8: Results from simulation on IASNFS pictured at May 20, 2010. The background is colored by sea surface speed, black dots represent surfaced particles, grey dots represent submerged plumes, and the magenta represents the EMPSR spill extent layers which is both filled-in behind and outlined over the particles for enhanced clarity.

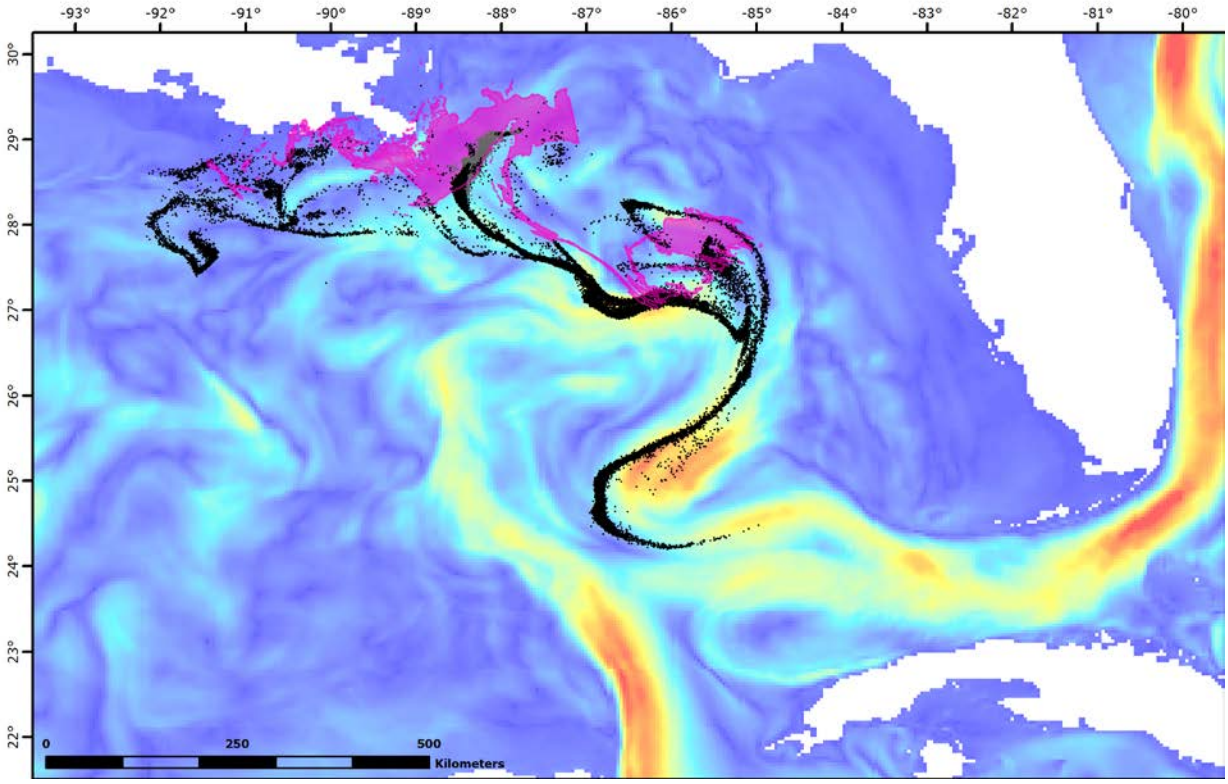

Figure 9: Results from simulation on GOM HYCOM pictured at May 20, 2010.

The presence of a submerged plume between 28–29°N trending south-southwest appears in both runs, corroborating the findings of Camilli et al. (2010) which observed a 35 km plume in the same region. Interestingly, IASNFS predicted a larger spread of the submerged plume than HYCOM, with a finger curling down and clockwise, as well as a plume trending northeast up De Soto Canyon, which separates the Mississippi-Alabama Shelf from the West Florida Shelf (Figure 10). The submerged plumes in both runs were composed of well over 4-million kg of crude on May 20, 2010, but only about 2% of the total spilled mass including all mass degraded. However BLOSOM was allowed to predict its own droplet-size distribution with the given blowout conditions and was not forced with dispersants, for which the maximum droplet-size was calculated at just over 5 mm. Given reports that the application of dispersants at the well-head pushed the maximum droplet-size down anywhere from 500 μm to 1 mm (Li et al., 2011), up to a 10-fold reduction, the mass of the submerged plume can be expected to significantly increase if the simulation parameters were adjusted for dispersants.

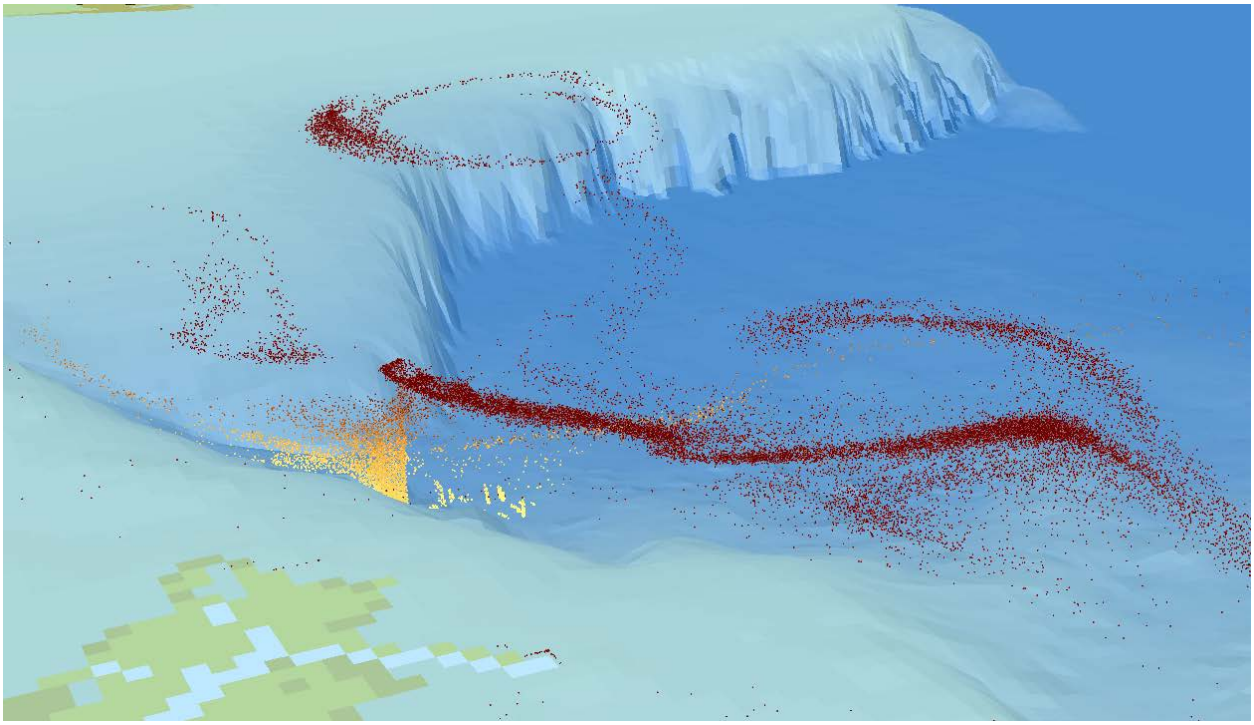

Figure 10: 3-D image of spill particles from IASNFS run on May 20, 2010 (same data as Figure 8) rendered in ArcScene. Image is looking southeast from Mississippi Delta; vertical exaggeration is set at 20; particles are colored from reddish-brown to bright yellow the deeper they are. Visible is the main rising jet/plume, the oil plume extending up De Soto Canyon (left), and an oil plume tail curling and extending south-southwest (towards viewer-right).

These results, especially juxtaposed, emphasize the sensitivities to ocean current data when modeling oil spills, which in a response scenario will be exacerbated having to use forecasts with potentially greater uncertainty and variance. Even when reinitializing and correcting spill extents with observations on regular intervals, the results vary due to differences in ocean current data, reinforcing the need for ensemble approaches whenever possible (Liu et al., 2011). In any scenario it would be best to run simulations on as many different hydrodynamic models as possible and make note of agreements and variances between results (e.g. Melsom et al., 2012), while using oil-spill observations (if available) to re-initialize the spill extents periodically, mitigating error growth (Liu et al., 2011).

7. CONCLUSIONS

As offshore operations move into increasingly deeper waters and challenging environments, the tools used to simulate offshore spills must keep pace with the amassed complexities and extreme conditions. Such constraints require modeling of jet-dynamics, submerged oil plumes, and integration of contrasting modeling approaches for the different regimes of the problem. BLOSOM addresses this need by merging and advancing the different models and approaches as components within an integrated and comprehensive blow-system modeling suite in a 3-D and spatially-explicit environment. New and effective means of merging various components grant BLOSOM exceptional power and adaptability in modeling the full fate of an oil spill, as exhibited by simulations of the Deepwater Horizon Spill with promising results, both in comparison to observed spill extents as well as corroborating measurements of the submerged oil plume.

Simulations provided in this report provide a great degree to robustness in simulations against real-world events, as well as shedding some light into the lesser known processes that may have occurred. Runs against the DWH Spill, while showing the dependence on and sensitivity to the provided hydrodynamic data, replicates real-world observations quite well both on the surface and with observations of the submerged plume and resulting fallout (Camilli et al., 2010; Valentine et al., 2014) without yet accounting for dispersant effects in the simulations. Further simulations with adjusted droplet-size distributions and different diffusion schemes may result in even more promising simulation capabilities.

Although BLOSOM was motivated in part to help support growing spill-response needs related to offshore energy exploration, particularly in deep and ultra-deep environments, it is also being employed to support spill-prevention and response-readiness (Nelson et al., 2015). By identifying trends and potential vulnerabilities related to oceanographic, climactic, engineering, and other considerations, BLOSOM supports informed decision-making, reduces uncertainties, and mitigates the potential of future spills to the benefit of stakeholders in industry, regulatory agencies, and research.

8. REFERENCES

Atlas, R. M. Microbial degradation of petroleum hydrocarbons: an environmental perspective. *Microbiological Reviews* **1981,** *45*, 180–209.

Baled, H.; Enick, R. M.; Wu, Y.; McHugh, M. A.; Burgess, W.; Tapriyal, D.; Morreale, B. D. Prediction of hydrocarbon densities at extreme conditions using volume-translated SRK and PR equations of state fit to high temperature, high pressure PVT data. *Fluid Phase Equilibria* **2012,** *317*, 65–76.

Bandara, U. C.; Yapa, P. D. Bubble Sizes, Breakup, and Coalescence in Deepwater Gas/Oil Plumes. *Journal of Hydraulic Engineering* **2011,** *137*, 729–738.

Brill, J. P.; Beggs, H. D. A Study of Two-Phase Flow in Inclinded Pipes. *Journal of Petroleum Technology* **1973,** *25*, 607–617.

Camilli, R.; Reddy, C. M.; Yoerger, D. R.; Van Mooy, B. A. S.; Jakuba, M. V.; Kinsey, J. C.; McIntyre, C. P.; Sylva, S. P.; Maloney, J. V. Tracking Hydrocarbon Plume Transport and Biodegradation at Deepwater Horizon. *Science* **2010,** *330*, 201–204.

Chang, A. F.; Pashikanti, K.; Liu, Y. A. Characterization, Physical and Thermodynamic Properties of Oil Fractions. *Refinery Engineering: Integrated Process Modeling and Optimization*; Wiley-VCH Verlag GmbH & Co. KGaA: Weinheim, DE, 2012.

Chen, F.; Yapa, P. D. Modeling gas separation from a bent deepwater oil and gas jet/plume. *Journal of Marine Systems* **2004,** *45*, 189–203.

Chen, F.; Yapa, P. D. Estimating the Oil Droplet Size Distributions in Deepwater Oil Spills. *Journal of Hydraulic Engineering* **2007,** *133*, 197–207.

Delvigne, G. A. L.; Sweeney, C. E. Natural dispersion of oil. *Oil & Chemical Pollution* **1988,** *4*, 281–310.

Durski, S. M. College of Earth, Ocean, and Atmospheric Sciences, Oregon State University. Personal communication, 2015.

Durksi, S. M. Vertical mixing schemes in the coastal ocean: Comparison of the level 2.5 Mellor-Yamada scheme with an enhanced version of the K profile parameterization. *Journal of Geophysical Research* **2004,** *109*, 1–23.

Englezos, P.; Kalogerakis, N.; Dholabhai, P. D.; Bishnoi, P. R. Kinetics of formation of methane and ethane gas hydrates. *Chemical Engineering Science* **1987a,** *42*, 2647–2658.

Englezos, P.; Kalogerakis, N.; Dholabhai, P. D.; Bishnoi, P. R. Kinetics of gas hydrate formation from mixtures of methane and ethane. *Chemical Engineering Science* **1987b,** *42*, 2659–2666.

Fay, J. A. Physical processes in the spread of oil on a water surface. Conference proceedings, Joint Conference for the Prevention and Control of Oil Spills, Washington, DC, 1971; p 463–467.

Fingas, M. A Review of Knowledge on Water-in-Oil Emulsions. Conference proceedings, International Oil Spill Conference, Savannah, GA, 2008.

Fingas, M.; Fieldhouse, B. Studies of the formation process of water-in-oil emulsions. *Marine Pollution Bulletin* **2003,** *47*, 369–96.

Fingas, M.; Fieldhouse, B. Formation of water-in-oil emulsions and application to oil spill modelling. *Journal of Hazardous Materials* **2004,** *107*, 37–50.

Fingas, M.; Fieldhouse, B. Studies on water-in-oil products from crude oils and petroleum products. *Marine Pollution Bulletin* **2012,** *64*, 272–83.

Fisher, H. B.; List, E. J.; Yikoh, R. C.; Imberger, J.; Brooks, N. H. *Mixing in Inland and Coastal Waters*; Academic Press, New York, NY, 1979.

Fofonoff, N. P.; Millard, R. C. *Algorithms for computation of fundamental properties of seawater*; UNESCO technical papers in marine science, Paris, France, 1983.

Gillespie, D. Exact numerical simulation of the Ornstein-Uhlenbeck process and its integral. *Physical Review E* **1996,** *54*, 2084–2091.

Heemink, A. W. Stochastic modelling of dispersion in shallow water. *Stochastic Hydrology and Hydraulics* **1990,** *4*, 161–174.

Johansen, Ø. DeepBlow - A Lagrangian Plume Model for Deep Water Blowouts. *Spill Science & Technology Bulletin* **2000,** *6*, 103–111.

Johansen, Ø. *Estimates of droplet size from subsea oil and gas leaks or blowouts*; SINTEF, Norway, 2002.

Johansen, Ø.; Brandvik, P. J.; Farooq, U. Droplet breakup in subsea oil releases – Part 2 : Predictions of droplet size distributions with and without injection of chemical dispersants. *Marine Pollution Bulletin* **2013,** *73*, 327–335.

Kesler, M. G.; Lee, B. I. Improved Prediction of Enthalpy of Fractions. *Hydrocarbon Processing* **1976,** *55*, 153–158.

King, M. B. *Phase Equilibrium in Mixtures*; Pergamon, Oxford, UK, 1969.

Le, M.; Kourafalou, V. H.; Paris, C. B.; Helgers, J.; Aman, Z. M.; Hogan, P. J.; Srinivasan, A. Surface Evolution of the Deepwater Horizon Oil Spill Patch: Combined Effects of Circulation and Wind-Induced Drift. *Environmental Science & Technology* **2012,** *46*, 7267–7273.

Lee, J. H. W.; Cheung, V. Generalized Lagrangian Model for Buoyant Jets in Currents. *Journal of Environmental Engineering* **1991,** *116*, 1085–1106.

Lehr, W. J. Review of modeling procedures for oil spill weathering behavior. Oil Spill Modeling and Process; Brebbia, C. A., Ed.; WIT Press: Southampton, UK, 2001.

Li, Z.; Lee, K.; Kepkey, P. E.; Mikkelsen, O.; Pottsmith, C. Monitoring dispersed oil droplet size distribution at the Gulf of Mexico Deepwater Horizon spill site. Conference proceedings, 2011 International Oil Spill Conference, Portland, OR, 2011; p 1–15.

Liu, Y.; Weisberg, R. H.; Hu, C.; Zheng, L. Trajectory Forecast as a Rapid Response to the Deepwater Horizon Oil Spill. *Monitoring and Modeling the Deepwater Horizon Oil Spill: A Record-Breaking Enterprise*; Liu, Y., Macfadyen, A., Ji, Z. G., Weisberg, R. H., Eds.; American Geophysical Union, 2011; p 153–165.

Mackay, D.; Shiu, W. Y.; Hossain, K.; Stiver, W.; McCurdy, D.; Petterson, S.; Tebeau, P. A. *Development and calibration of an oil spill behavior model*; United States Coast Guard Office of Research and Development, Groton, CT, 1982.

Madsen, O. S. A Realistic Model of the Wind-Induced Ekman Boundary Layer. *Journal of Physical Oceanography* **1977,** *7*, 248–255.

McNutt, M. K.; Camilli, R.; Crone, T. J.; Guthrie, G. D.; Hsieh, P. A.; Ryerson, T. B.; Savas, O.; Shaffer, F. "Review of flow rate estimates of the Deepwater Horizon oil spill. *Proceedings of the National Academy of Sciences* **2011,** *109*, 20260–20267.

Melsom, A.; Counillon, F.; LaCasce, J. H.; Berting, L. Forecasting search areas using ensemble ocean circulation modeling. *Ocean Dynamics* **2012,** *62*, 1245–1257.

Nelson, J. R.; Grubesic, T. H.; Sim, L.; Rose, K.; Graham, J. Approach for assessing coastal vulnerability to oil spills for prevention and readiness using GIS and the Blowout and Spill Occurrence Model. *Ocean & Coastal Management* **2015,** *112*, 1–11.

North, E. W.; Adams, E. E.; Schlag, Z.; Sherwood, C. R.; He, R.; Hyun, K. H.; Socolofsky, S. A. Simulating Oil Droplet Dispersal From the Deepwater Horizon Spill With a Lagrangian Approach. *Monitoring and Modeling the Deepwater Horizon Oil Spill: A Record-Breaking Enterprise*; American Geophysical Union: Washington, DC, 2011; p 217–226.

Oreskes, N. The Role of Quantative Models in Science in Models in Ecosystem Science. *Models in Ecosystem Science*; Canham, C. D., Cole, J. J., Lauenroth, W. K., Eds.; Princeton University Press: Princeton, NJ, 2010; p 13–31.

Oreskes, N.; Shrader-Frechette, K.; Belitz, K. Verification, validation, and confirmation of numerical models in the earth sciences. *Science* **1994,** *263*, 641–646.

Reed, M.; Johansen, Ø.; Brandvik, P. J.; Daling, P.; Lewis, A.; Fiocco, R.; Mackay, D.; Prentki, R. Oil Spill Modeling towards the Close of the 20th Century: Overview of the State of the Art. *Spill Science & Technology Bulletin* **1999,** *5*, 3–16.

Reinhart, R.; Rose, R. Evaporation of Crude Oil at Sea. *Water Research* **1982,** *16*, 1325–1335.

Riazi, M. R.; Roomi, Y. A. A model to predict rate of dissolution of toxic compounds into seawater from an oil spill. *International Journal of Toxicology* **2008,** *27*, 379–86.

Rye, H.; Brandvik, P. J. Verification of Subsurface Oil Spill Models. Conference proceedings, International Oil Spill Conference, Fort Lauderdale, FL, 1997; p 551–557.

Rye, H.; Brandvik, P. J.; Reed, M. Subsurface oil release field experiment-observations and modeling of subsurface plume behavior. Conference proceedings, 19th Arctic and Marine Oil Spill Program Technology Seminar, Ottawa, Canada, 1996; pp 1417–1435.

Schatzmann, M. Calculation of submerged thermal plumes discharged into air and water flows. Conference proceedings, 19th International Association for Hydro-Environment Engineering and Research Congress, Delft, Netherlands, 1979; p 239–246.

Sharqawy, M. H.; Lienhard V. J. H.; Zubair, S. M. Thermophysical properties of seawater: a review of existing correlations and data. *Desalination and Water Treatment* **2010,** *16*, 354–380.

Shen, H. T.; Yapa, P. D.; Petroski, M. E. A Simulation Model for Oil Slick Transport in Lakes. *Water Resources Research* **1987,** *23*, 1949–1957.

Smagorinsky, J. General circulation experiments with the primitive equations I. The basic experiment. *Monthly Weather Review* **1963,** *91*, 99–164.

Sterman, J. D.; Rykiel, E. J.; Oreskes, N.; Belitz, K.; Shrader-Frechette, K. The meaning of models. Science **1994,** *264*, 329–330.

Stiver, W.; Mackay, D. Evaporation rate of spills of hydrocarbons and petroleum mixtures. *Environmental Science and Technology* **1984,** *18*, 834–840.

Twu, C. H. An Internal Consistent Correlation for Predicting the Critical Properties and Molecular Weights of Petroleum and Coal Tar Liquids. *Fluid Phase Equilibria* **1984,** *16*, 137–150.

Valentine, D. L.; Fisher, G. B.; Bagby, S. C.; Nelson, R. K.; Reddy, C. M.; Sylva, S. P.; Woo, M. A. Fallout plume of submerged oil from Deepwater Horizon. *Proceedings of the National Academy of Sciences* **2014,** *111*, 1–6.

Wang, S.; Shen, Y. M.; Zheng, Y. Two-dimensional numerical simulation for transport and fate of oil spills in seas. *Ocean Engineering* **2005,** *32*, 1556–1571.

Yapa, P. D.; Zheng, L. Simulation of Oil Spills From Underwater Accidents I: Model Development. *Journal of Hydraulic Research* **1997,** *35*, 673–687.

Yapa, P. D.; Zheng, L.; Chen, F. A Model for Deepwater Oil/Gas Blowouts. *Marine Pollution Bulletin* **2001,** *43*, 234–241.

Yapa, P. D.; Zheng, L.; Nakata, K. Modeling Underwater Oil/Gas Jets and Plumes. *Journal of Hydraulic Engineering* **1999,** *125*, 481–491.

Zheng, L.; Yapa, P. D. Buoyant Velocity of Spherical and Nonspherical Bubbles/Droplets. *Journal of Hydraulic Engineering* **2000,** *126*, 852–854.

Zheng, L.; Yapa, P. D. Modeling gas dissolution in deepwater oil/gas spills. *Journal of Marine Systems* **2002,** *31*, 299–309.

Zheng, L.; Yapa, P. D.; Chen, F. A model for simulating deepwater oil and gas blowouts – Part I: Theory and model formulation. *Journal of Hydraulic Research* **2002,** *41*, 339–351.

APPENDIX A: CONTROL-VOLUME AND ENTRAINMENT

The governing equations for mass and velocity are given as follows, where each velocity component is calculated separately for each scalar component.

$$m_{k+1} = m_k + m_Q - m_L$$

$$\mathrm{v}'_{\mathrm{n}+1} = \frac{(m_n - m_L)\mathrm{v}_\mathrm{n} + m_Q \mathrm{v}_\mathrm{a}}{m_{n+1}} + \frac{\Delta\rho}{\rho_n} g t \boldsymbol{k}$$

$$\mathrm{v}_{\mathrm{n}+1} = \mathrm{v}'_{\mathrm{n}+1} + (1 - j^2)(\mathrm{v}_\mathrm{a} + w_b \boldsymbol{k} - \mathrm{v}'_{\mathrm{n}+1})$$

Conservation of heat ignores heat diffusivity, as it was determined a very minimal component through sensitivity testing. Heat and salinity are both calculated with the following equations where I can represent the specific heat or salinity.

$$I'_{n+1} = \frac{(m_n - m_L)I_n + m_Q I_a}{m_{n+1}}$$

$$I_{n+1} = I'_{n+1} + (1 - j^2)(I_a - I'_{n+1})$$

The height of the control-volume is calculated from the previous displacement length as a ratio of the change in velocity, regulated by the jet-coefficient. The radius is simply calculated from rearranging the formula for the volume of a cylinder using the given height, mass, and density; where Φ is the elevation angle of the control-volume's velocity vector.

$$h_{n+1} = h_n + j(\vec{\mathbf{v}}_{n+1} t \sin\Phi - h_n)$$

$$r_{n+1} = \sqrt{\frac{V_{n+1}}{\pi h_{n+1}}}$$

The volume flux from sheer entrainment is calculated from the surface area of the control-volume's sides, the difference between the velocity of the control-volume from the ambient velocity projected onto the same direction, and a shear entrainment coefficient (α) based on the Froude number (Fr), a number that is used to characterize the resistance of an object moving through water. The equations as adopted from Schatzmann (1979) by Lee and Cheung (1991) are below.

$$\frac{dQ_s}{dt} = 2\pi r h \alpha \mathrm{v}_s$$

$$\alpha = \mathrm{v}_\mathrm{s}\sqrt{2}\frac{0.057 + 0.554 \sin(\Phi)\, Fr^{-2}}{1 + 5\, \vec{\mathbf{v}}'_\mathrm{a}/\mathrm{v}_\mathrm{s}}$$

$$Fr = E\frac{\mathrm{v}_\mathrm{s}}{\sqrt{rg\,\Delta\rho/\rho}}$$

$$\mathrm{v}_s = |\vec{\mathbf{v}} - \vec{\mathbf{v}}'_a|$$

where E is a proportionality constant in the model assumed to be 2.0 (Yapa and Zheng, 1997), and v_s is a shear velocity based on the difference from the control-volume's velocity vector ($\vec{\mathbf{v}}$) from the ambient velocity vector projected onto the former ($\vec{\mathbf{v}}'_a$). The volume flux from forced

entrainment is calculated as the apparent surface area of the sides of the control-volume element to the ambient current, expanded by the difference between the velocity and ambient velocity in that direction. They are simplified from the original equations in Lee and Cheung (1991) due to the simpler geometry of shearing control-volumes.

$$\frac{dQ_{fx}}{dt} = |u - u_a| \cdot 2rh$$

$$\frac{dQ_{fy}}{dt} = |v - v_a| \cdot 2rh$$

$$\frac{dQ_{fz}}{dt} = |w - w_a| \cdot \pi r \Delta r$$

where Δr is radius growth during the last timestep and u, v, z denote zonal, meridional, and vertical velocities with subscript a for the ambient.

APPENDIX B: DROPLET-SIZES AND TERMINAL BUOYANT VELOCITY

The median droplet-size (δ_{50}) and droplet-size distributions are calculated using the following methods (Johansen et al., 2013).

$$We^* = We\left[1 + B\frac{We}{Re}\left(\frac{\delta_{50}}{d_0}\right)^{1/3}\right]^{-1}$$

$$\delta_{50}/d_0 = AWe^{*-0.6}$$

Where d_0 is the diameter of the blowout, We is the Weber number, We^* is the modified Weber number, Re is the Reynolds number, and A and B are coefficients currently set to 16.5 and 0.8. As the peak droplet-size is implicit in the equation, it must be solved iteratively. The Weber number and Reynolds numbers must be calculated from a modified exit velocity ($\vec{\mathbf{v}}_E$) based on the Froude number (Fr) and void ratio (n) (ratio of the volume gases to the total volume).

$$We = \rho\vec{\mathbf{v}}_E^2 d_0/\sigma$$

$$Re = \rho\vec{\mathbf{v}}_E d_0/\mu$$

$$\vec{\mathbf{v}}_n = \vec{\mathbf{v}}_0/\sqrt{1-n}$$

$$Fr = \vec{\mathbf{v}}_n/\sqrt{d_0 g\Delta\rho/\rho_a}$$

$$\vec{\mathbf{v}}_E = \vec{\mathbf{v}}_n(1 + Fr^{-1})$$

where $\vec{\mathbf{v}}_0$ is the exit velocity of the oil; dynamic viscosity (μ) and density (ρ) values are of the liquid portion of the jet; and the interfacial-tension (σ) is for the oil-water interface.

Droplet-size distribution is calculated for the volume of all droplets up to the calculated droplet-size.

$$V(\delta) = 1 - exp[-0.693\left(\delta/_{\delta_{50}}\right)^{1.8}]$$

To calculate the terminal droplet buoyancy (w_b), a three-phase approach for spherical, ellipsoidal, and spherical-cap droplet shapes (in order of increasing size regimes) is used as described in Zheng and Yapa (2000). This replaces the formally two-phase approach of spherical and ellipsoidal alone and provides greater accuracy for larger droplet sizes. The method described can be applied to any liquid and gas droplet/bubble and thus, the methods described can be applied both to the crude oil droplets and gas bubbles in the control-volume.

All droplets/bubbles with a diameter of 1 mm or less are assumed to be spherical in shape and act like rigid particles. Their terminal velocity is obtained by using the equation below.

$$w_b = \frac{Re \cdot \mu}{\rho\delta}$$

with the Reynolds number calculated as follows.

$$N_D = \frac{4\rho\Delta\rho g\delta^3}{3\mu^2}$$

$$W = \log N_D$$

$$\begin{pmatrix} Re = \frac{N_D}{24} - 1.7569x10^{-4}N_D^2 + 6.9252x10^{-7}N_D^3 - 2.3027x10^{-10}N_D^4 & if\ N_D \leq 73 \\ \log Re = -1.7095 + 1.33438W - 0.11591W^2 & if\ N_D \leq 580 \\ \log Re = -1.81391 + 1.34671W - 0.12427W^2 + 0.006344W^3 & if\ N_D > 580 \end{pmatrix}$$

In the ellipsoidal shape, defined as between 1 mm diameter and the critical diameter (δ_c), the terminal velocity is determined by the Morton number (Mo) and the Eötvös number (Eo).

$$Mo = g\mu_{pw}^4 \left(\frac{\Delta\rho}{\rho^2}\right)\sigma$$

$$Eo = g\Delta\rho\delta^2/\sigma$$

$$H = \frac{4}{3}EoMo^{-0.149}\left(\frac{\mu}{\mu_{pw}}\right)^{-0.14}$$

$$J = 0.94H^{0.757} \quad if\ 2 < H \leq 59.3$$
$$J = 3.42H^{0.441} \quad if\ H > 59.3$$

$$w_b = \frac{\mu}{\rho\delta}Mo^{-0.149}(J - 0.857)$$

where μ_{pw} is the viscosity of pure water at ambient temperature and pressure.

If the droplet or bubble is larger than the critical diameter (δ_c), it is assumed to be spherical-cap in shape and the terminal velocity governed almost solely by the densities of the droplet/bubble and the ambient fluid. To obtain the critical diameter, an approximation method for where the terminal velocities for the ellipsoidal shape and spherical-cap shape coincide, as proposed by Zheng and Yapa (2000), is used.

$$w_b = 0.711\sqrt{g\delta\Delta\rho/\rho}$$

$$\log \delta_c = \frac{b_1 - b_2}{0.5 - a}$$

$$a = \frac{y_2 - y_1}{x_1 - x_2}$$

$$b_1 = \log(0.711\sqrt{g\Delta\rho/\rho})$$

$$b_2 = y_1 - ax_1$$

where the set (x_1, y_1) represents a point equivalent to $(\log \delta_e\ ,\ \log w_b)$ when $H = 59.3$; and (x_2, y_2) represents a point equivalent to $(\log \delta_e\ , \log w_b)$ when $\delta_e$is equal to 15 mm in the ellipsoidal regime. As the critical diameter calculations do not need to be recalculated every timestep, one of a number of conditions must be met in the model to necessitate recalculating the critical diameter so as to maintain a high level of efficiency: either having not yet been calculated, surpassing a maximum timestep interval since last calculation, or significant changes in the viscosity or densities of either the droplet/bubble or ambient seawater.

APPENDIX C: TURBULENT DIFFUSION

Appendix C was added to this paper after the final revisions by coauthors, several mistakes in this appendix were subsequently found. Please disregard the Appendix C and refer to the technical report by Duran (2016) for the diffusion schemes used in BLOSOM.

Duran, R. *Sub-Grid Parameterizations for Oceanic Oil-Spill Simulations*; NETL-TRS-9-2016; EPAct Technical Report Series; U.S. Department of Energy, National Energy Technology Laboratory: Albany, OR, 2016; p 36.

Random-walk for spill modeling is based on Fisher et al. (1979) wherein a random diffusion velocity is added to every particle at each timestep as a function of a random number generator and the diffusivity. It is the simplest of the methods as a zeroth-order Markov model with each step being completely independent.

$$\mathrm{v}_t = \omega\sqrt{0.5K_{EKE}}$$

$$\vec{\mathbf{v}}_{\boldsymbol{t}} = 2\omega\sqrt{K_S/t}$$

where ω represents a Gaussian-distributed random number of variance 1, and each instance of ω is independently generated. The first equation is applied for each horizontal scalar if using eddy kinetic energy (EKE) values for diffusivity, or the second equation for eddy viscosity, applied to the total magnitude and given a random perturbation from the current azimuth with a Gaussian distribution of mean 0 and standard deviation of π radians.

Random-flight (Heemink, 1990) is a first-order Markovian processes that incorporates memory in the velocity perturbations, scaled by a Lagrangian timescale (τ). It is applied to each scalar, regardless if deriving diffusivity from eddy kinetic or eddy viscosity values.

$$\frac{d\mathrm{v}_t}{dt} = -\left(1 - \frac{t}{\tau}\right)\mathrm{v}_t + \frac{t}{\tau}\mathrm{v}_t'\omega$$

$$\mathrm{v}_t' = K_{EKE}$$

$$\mathrm{v}_t' = \sqrt{2K_S/t}$$

The hybrid approach incorporates a first-order Markovian process for the magnitude of the diffusive velocity, much like the random flight model, but with the directional component perturbed by independent increments not tied to the time scale.

$$\frac{d\vec{\mathbf{v}}_{\boldsymbol{t}}}{dt} = -\left(1 - \frac{t}{\tau}\right)\vec{\mathbf{v}}_{\boldsymbol{t}} + \frac{t}{\tau}\vec{\mathbf{v}}_t'\omega$$

$$\vec{\mathbf{v}}_t' = K_{EKE}\sqrt{2}$$

$$\vec{\mathbf{v}}_t' = 2\sqrt{K_S/t}$$

$$\frac{d\theta}{dt} = \pi\,\omega$$

When eddy diffusivity is used, a simple Euler method assuming a quasi-steady state can be assumed for each timestep. When using EKE values for any method besides random-walk however, the added velocity must be treated as a stochastic differential, which may be solved either through an exact numerical solution as given by Gillespie (1996) for the case of random-flight or statistically estimated by providing the random Gaussian term with a standard deviation, based on the expected standard deviation if solving with a much more precise solution timestep (t_s), usually set at 1 second. As the variance of the instantaneous added velocity is simply a sum of the variances at each solution timestep interval, the variance of the resulting distance can be calculated similarly as a summation function, which may then be divided by the timestep to give the standard deviation of the average diffusive velocity over the timestep, and divided by the diffusive velocity term to give the expected standard deviation of the random term.

$$\mathrm{stdev}(dist) = t_s \mathrm{v}'_t \sum_{i=0}^{t/t_s} \sqrt{i} = \frac{2\mathrm{v}'_t t^{1.5}}{3{t_s}^{0.5}}$$

$$\mathrm{stdev}(\omega) = \frac{2}{3}\sqrt{{}^{t}/_{t_s}}$$

Thus for random-flight or random-hybrid methods, when using EKE values, the random term (ω) is instead given a standard deviation as denoted above. However this does not apply to random-walk or the directional perturbation component of the hybrid method, which may continue to be solved with the Euler method.

APPENDIX D: WEATHERING MODELS

BLOSOM employs a hybrid of evaporation equations proposed by Stiver and Mackay (1984) and Reinhart and Rose (1982), which are calculated for each pseudo-component at each timestep.

$$\frac{dX_i}{dt} = -\gamma X_i^{0.5} M_{\boldsymbol{i}} P_{\boldsymbol{v}(\boldsymbol{i})} S_i^{-0.67}$$

where X_i is the mass remaining per unit area (kg m^{-2}) of the i-th pseudo-component; γ is a mass transfer coefficient; $M_{\boldsymbol{i}}$ is the molar mass of the pseudo-component in kg per mol; $P_{\boldsymbol{v}(\boldsymbol{i})}$ is the vapor pressure of the pseudo-component in Pascal; and S_i is the Schimdt number of the pseudo-component. The mass transfer coefficient is calculated as follows

$$\gamma = \frac{420\vec{\mathbf{v}}_w^{0.78} d^{-0.11}}{e^{180h}\rho RT}$$

where $\vec{\mathbf{v}}_w$ is the surface wind speed; d is the diameter of the portion of the slick represented by the parcel; h is the thickness of the slick in meters; ρ is the total density of the crude and emulsion; R is the gas-constant; and T is the temperature in Kelvin.

Emulsification first assigns a stability class based on the density, viscosity, and resin and asphaltenes contents of the total crude, with each class having a stable water content value (Fingas and Fieldhouse, 2004; Fingas, 2008). The class is assigned by calculating the class number and determining whether it falls between the low and high values for the emulsification classes outlined in the following table.

Class	Low Value	High Value	A	B	Stable Water Content
Unstable	$-\infty$	0.615	0	0	0.06
Mesostable	0.615	0.66	2820	2946	0.66
Stable	0.66	∞	2160	435	0.8
Entrained	0.64	0.72	1848	1098	0.46

$$\text{density parameter } (D) = \begin{pmatrix} 0.97 - \frac{\rho}{1000} & if\ \frac{\rho}{1000} < 0.97 \\ 0.97 & if\ \frac{\rho}{1000} = 0.97 \\ \frac{\rho}{1000} - 0.97 & if\ \frac{\rho}{1000} > 0.97 \end{pmatrix}$$

$$\text{viscosity parameter } (V) = \begin{pmatrix} 8.7 - \ln\mu & if\ \ln\mu < 8.7 \\ 8.7 & if\ \ln\mu = 8.7 \\ \ln\mu - 8.7 & if\ \ln\mu > 8.7 \end{pmatrix}$$

$$\text{resin parameter } (R) = \begin{pmatrix} 20 & if\ \%_{resin} = 0 \\ 5.4 - \%_{resin} & if\ \%_{resin} < 5.4 \\ \%_{resin} - 5.4 & if\ \%_{resin} > 5.4 \end{pmatrix}$$

$$\text{asphaltene parameter } (A) = \begin{pmatrix} 30 & if\ \%_{asphaltene} = 0 \\ 12 - \%_{asphaltene} & if \%_{asphaltene} < 12 \\ \%_{asphaltene} - 12 & if\ \%_{asphaltene} > 12 \end{pmatrix}$$

$$\text{class number} = 0.738 - 0.197D - 0.0126V - 0.0007R - 0.00358A$$

The entrained and stable state overlap, but the emulsion is considered entrained if the density of the crude oil is greater than 960 kg m^{-3} and the viscosity of the crude oil is greater than 10 Pa·s. Resins and asphaltenes are assumed not to degrade, and consequently, their fraction increases with an increase in the fraction degraded, changing the resulting emulsification class likely to result. The time for formation is estimated from the A and B parameters from the above table and local wave height (w_h).

$$\text{Time to formation } (s) = A + \frac{B}{h_w^{1.5}}$$

Dispersion is calculated using the methods from Delvigne and Sweeney (1988) where dispersion amounts are calculated for some droplet-size interval. Calculating dispersion requires the significant wave height (h_w), wave period (T_h), the wave energy (Q_w), and fractional area covered in breaking waves (f_{bw}), many of which can be correlated from each other and the surface wind conditions if not provided in the hydrodynamic files.

$$Q_{disp} = 4450(\mu/\rho)^{-0.4} Q_w^{0.57} f_{bw} \delta_{di} \Delta\delta$$

where Q_{disp} is the volume displaced per slick surface area for the droplet-diameter interval; μ/ρ is the kinematic viscosity of the crude; δ_{di} is the mean diameter; and $\Delta\delta$ is the diameter interval. In practice, as BLOSOM simply calculates dispersion only for the particles that never surface, the diameter interval is equivalent to the maximum droplet-size for those entrained droplets which never surface, and the mean diameter is half that. All components are assumed to have dispersed equally under the well-mixed assumption.

Dissolution is calculated for each pseudo-component, similar to evaporation, based on the methods of Riazi and Roomi (2008) to calculate the volume fraction dissolved for the pseudo-component (f_i^{dis}).

$$f_i^{dis} = -\left[1 - \exp\left(Q_i^{dis} t\right)\right]$$

$$Q_i^{dis} = \frac{K_i \cdot C_i}{\delta \rho_i^{mol}}$$

$$K_i = \frac{4.18 \times 10^{-9} T^{0.67}}{V_{mol}^{0.4} A_i^{0.1}}$$

where Q_i^{dis} is the mass transfer coefficient of the i-th pseudo-component; C_i is the solubility of the pseudo-component in mol/L; ρ_i^{mol} is the molar density of the pseudo-component in mol m^{-3};

$V_{mol}^{0.4}$ is the molar volume of the pseudo-component at boiling in m^3mol^{-1}; and A_i is the surface area, estimated from the droplet-size and number of droplets proportioned by the volume fraction of the pseudo-component. Solubility is estimated using an empirical fit modified from the original given in Riazi and Roomi (2008).

$$C_i = \exp\left[10 - 0.003M_i^2 + 0.23M_i - (0.01 + 1.8\text{x}10^{-4}M_i)S - 4250/T\right]$$

where M_i is the molar mass of the pseudo-component in g/mol and S is the salinity of the ambient water in PSU. Past a molar mass of 300 g/mol, the solubility is effectively assumed to be 0. Likewise, the fit is assumed to be accurate only above molar masses 80 g/mol or more and any cuts less than that will be assumed a molar mass of 80. If a fraction of aromatics is provided for the cut data, the solubility of the aromatic fraction is estimated based off an empirical fit to the solubility of naphthalene, adjusted by relative molar mass compared with the molar mass of naphthalene.

$$C_{aromatics} = 5\text{x}10^{-9}e^{0.036T}\exp[1.0\text{x}10^{-5}(128.17 - M_i)^3]$$

The total solubility is simply assumed to be a mean of the calculated solubility and the naphthalene solubility based on the fraction of aromatics. However aromatics are assumed to preferentially degrade, so the assumed remaining fraction of aromatics is subtracted by the total fraction degraded. Once the fraction degraded is equal to or greater than the fraction of aromatics given, this no longer comes into play.

When surfaced, degradation is assumed to preferentially thin the thickness of the slick represented by the parcel rather than shrink the radius until reaching some minimum thickness. Meanwhile, increases in volume (e.g. from emulsification) only increase the slick's thickness. Meanwhile some thinning and spreading of the slick also occurs due to spreading. Both the minimum thickness and spreading models are adapted from Fay (1971) assuming the gravity-viscous spreading regime is always the dominant one.

This page intentionally left blank.

Jared Ciferno
Director
Strategic Center for Natural Gas and Oil
National Energy Technology Laboratory
U.S. Department of Energy

Maria Vargas
Deputy Director
Strategic Center for Natural Gas and Oil
National Energy Technology Laboratory
U.S. Department of Energy

Roy Long
Technology Manager
Strategic Center for Natural Gas and Oil
National Energy Technology Laboratory
U.S. Department of Energy

Elena Melchert
Program Manager
Oil and Gas Production
Office of Fossil Energy
U.S. Department of Energy

Cynthia Powell
Director
Office of Research and Development
National Energy Technology Laboratory
U.S. Department of Energy

Mark Williams
RES Program Manager
URS Corporation